

MODELING *Kepler* TRANSIT LIGHT CURVES AS FALSE POSITIVES: REJECTION OF BLEND SCENARIOS FOR KOI-377, AND STRONG EVIDENCE FOR A SUPER-EARTH-SIZE PLANET IN A MULTIPLE SYSTEMGUILLERMO TORRES<sup>1</sup>, FRANÇOIS FRESSIN<sup>1</sup>, NATALIE M. BATALHA<sup>2</sup>, WILLIAM J. BORUCKI<sup>3</sup>, TIMOTHY M. BROWN<sup>4</sup>, STEPHEN T. BRYSON<sup>3</sup>, LARS A. BUCHHAVE<sup>5</sup>, DAVID CHARBONNEAU<sup>1</sup>, DAVID R. CIARDI<sup>6</sup>, EDWARD W. DUNHAM<sup>7</sup>, DANIEL C. FABRYCKY<sup>1</sup>, ERIC B. FORD<sup>8</sup>, THOMAS N. GAUTIER III<sup>9</sup>, RONALD L. GILLILAND<sup>10</sup>, MATTHEW J. HOLMAN<sup>1</sup>, STEVE B. HOWELL<sup>11</sup>, HOWARD ISAACSON<sup>12</sup>, JON M. JENKINS<sup>13</sup>, DAVID G. KOCH<sup>3</sup>, DAVID W. LATHAM<sup>1</sup>, JACK J. LISSAUER<sup>3</sup>, GEOFFREY W. MARCY<sup>14</sup>, DAVID G. MONET<sup>15</sup>, ANDREJ PRSA<sup>16</sup>, DARIN RAGOZZINE<sup>1</sup>, JASON F. ROWE<sup>3,17</sup>, DIMITAR D. SASSELOV<sup>1</sup>

Draft version November 7, 2018

## ABSTRACT

The high-precision light curves from the *Kepler* mission contain valuable information on the nature of the phenomena producing the transit-like signals. To assist in exploring the possibility that they are the result of an astrophysical false positive, we describe a procedure we refer to as **BLENDER** to model the photometry not in terms of a planet orbiting a star, but instead as a “blend”. A blend may consist of a background or foreground eclipsing binary (or star-planet pair) whose eclipses are attenuated by the light of the candidate and possibly other stars within the photometric aperture. We apply the technique to the case of KOI-377, a particularly interesting *Kepler* target harboring two previously confirmed Saturn-size planets (*Kepler*-9 b and *Kepler*-9 c) showing transit timing variations, and an additional shallower signal with a 1.6-day period that would correspond to a super-Earth with a radius of  $1.4 R_{\oplus}$ , the smallest yet discovered. Using **BLENDER** together with constraints from high-resolution imaging, spectroscopy, and astrometry (centroid motions), we are able to rule out all blends for the two deeper signals and provide independent validation of their planetary nature. For the shallower signal we rule out a large fraction of the false positive scenarios that might mimic these transit-like events. The false alarm rate (FAR) for remaining blends depends in part (and inversely) on the unknown frequency of small-size planets. Our most conservative (smallest) estimates of this frequency lead to a FAR of  $5.9 \times 10^{-3}$ , implying a high likelihood that the signal is due to a super-Earth-size planet rather than a false positive.

*Subject headings:* binaries: eclipsing — planetary systems — stars: individual (KOI-377, *Kepler*-9)  
— stars: statistics

## 1. INTRODUCTION

The *Kepler* mission, launched in March of 2009, was designed to address the important question of the frequency of Earth-size planets around Sun-like stars, and to characterize extrasolar transiting planets through a 3.5-year program of very precise photometric monitoring of  $\sim 156\,000$  stars (Koch et al. 2010). Science results from the mission have already begun to appear (Borucki et al. 2010a,b; Steffen et al. 2010). As shown already by ground-based surveys for transiting planets,

considerable effort is required to validate candidates detected photometrically. This is because false positives usually outnumber true planetary systems by a large factor, which is about 10:1 for the most successful surveys from the ground, but is not yet well characterized for *Kepler*. The follow-up efforts by the *Kepler* team have been summarized by Batalha et al. (2010).

Spectroscopy is often a crucial step in the vetting process, as it allows not only to measure the mass of a planet but also to examine any changes in the line profiles (bisector spans) that might indicate a false positive (see Queloz et al. 2001; Torres et al. 2005). Some of the most challenging false positives to rule out include chance alignments with a background eclipsing binary (“blends”). However, for faint candidates ( $V > 14$ ) high-resolution, high signal-to-noise ratio spectroscopy becomes prohibitively expensive in terms of telescope time. Even for brighter candidates, the reflex motion of the star due to an Earth-mass planet can sometimes be below the radial-velocity detection limit, making spectroscopic confirmation very difficult or impossible. The question then becomes how to validate these candidates, particularly the ones with small planets that are precisely among the most interesting.

A number of other tests have been developed that can aid in understanding the nature of the candidate, and that rely on the long-term and nearly continuous photometric monitoring of *Kepler*, as well as the very high astrometric precision achieved in determining the cen-

<sup>1</sup> Harvard-Smithsonian Center for Astrophysics, Cambridge, MA 02138, e-mail: gtorres@cfa.harvard.edu

<sup>2</sup> San Jose State University, San Jose, CA 95192

<sup>3</sup> NASA Ames Research Center, Moffett Field, CA 94035

<sup>4</sup> Las Cumbres Observatory Global Telescope, Goleta, CA 93117

<sup>5</sup> Niels Bohr Institute, Copenhagen University, DK-2100 Copenhagen, Denmark

<sup>6</sup> NASA Exoplanet Science Institute/Caltech, Pasadena, CA USA 91125

<sup>7</sup> Lowell Observatory, Flagstaff, AZ 86001

<sup>8</sup> University of Florida, Gainesville, FL 32611

<sup>9</sup> Jet Propulsion Laboratory/California Institute of Technology, Pasadena, CA 91109

<sup>10</sup> Space Telescope Science Institute, Baltimore, MD 21218

<sup>11</sup> National Optical Astronomy Observatory, Tucson, AZ 85719

<sup>12</sup> San Francisco State University, San Francisco, CA 94132

<sup>13</sup> SETI Institute/NASA Ames Research Center, Moffett Field, CA 94035

<sup>14</sup> University of California, Berkeley, CA 94720

<sup>15</sup> US Naval Observatory, Flagstaff Station, Flagstaff, AZ 86001

<sup>16</sup> Villanova University, Villanova, PA 19085

<sup>17</sup> NASA Postdoctoral Program Fellow

troids of the stars (see also Steffen et al. 2010). These tests include: *i*) verifying that alternating events have the same depth, which they may not if the signal is due to a background eclipsing binary; *ii*) checking for the presence of shallow secondary eclipses, which are common in eclipsing binaries but are not expected for the smallest planets; *iii*) checking for ellipsoidal variations, which could be another sign of a blend. *iv*) checking for changes in the centroid positions correlated with the brightness changes, which, if detected, might indicate a blend, or at the very least, a crowded aperture. This is a powerful diagnostic that is able to disprove many background blends.

In addition to these tests, high-resolution imaging is an important tool to identify neighboring stars that might be eclipsing binaries with the potential to cause the transit-like signals. The photometric aperture of *Kepler* is large enough (typically many arc seconds across) that it usually includes other stars in addition to the candidate, which increases the risk of such blends. In some cases, near-infrared observations with Warm *Spitzer* can allow one to reject the planet hypothesis if the transit depth at  $3.6\,\mu\text{m}$  or  $4.5\,\mu\text{m}$  is significantly different from that in the *Kepler* band. Such a signature might result from a blend with an eclipsing binary of a different spectral type than the candidate.<sup>18</sup>

Even with this extensive battery of tests it may still be difficult or impossible to provide validation for many of the most interesting planet candidates discovered by *Kepler*. For example, blend scenarios involving an eclipsing binary or an eclipsing star-planet pair physically associated with the candidate (hierarchical triple systems) and in a long-period orbit around their common center of mass would often be spatially unresolved from the ground. These configurations may not be detectable spectroscopically either, and would likewise not produce any measurable centroid motion. Therefore, it is imperative to take advantage of all the information available in vetting candidates.

With this as our motivation, we describe here the use of the *Kepler* light curves themselves in a different way to help discriminate between true planetary transits and a large variety of possible blend scenarios, on a much more quantitative basis than simple back-of-the-envelope calculations could provide. The technique tests these scenarios by directly modeling the light curves as blends, and has considerable predictive power that allows the expected properties of the various configurations to be tested against other information that may be available. Both hierarchical triples and background blends can be explored. A restricted application of this type of modeling to *Kepler* has already been made for the five multi-planet candidates announced recently by Steffen et al. (2010). For the present paper we have chosen to illustrate the full potential of the method, which we refer to as **BLENDER**, by applying it to the unique case of *Kepler* Object of Interest 377 (KOI-377). This is a multi-planet system reported and described in detail by Holman et al. (2010), with *three* low-amplitude periodic signals in its

light curve. We have selected this system for two main reasons. On the one hand, it represents the first unambiguous detection of transit timing variations (TTVs) in an extrasolar planet, with a pattern of variation seen in two of its signals (*Kepler*-9 b and *Kepler*-9 c) that constitutes irrefutable evidence that the objects producing them are bona-fide planets. This offers an ideal opportunity to test **BLENDER** because their true nature is already known. On the other hand, the third signal (KOI-377.03) is small enough that it would correspond to a super-Earth, but validation of its planetary origin is not yet in hand. Should it be validated, *Kepler*-9 would become an even more remarkable laboratory for the study of the architecture of planetary systems involving small planets. Thus, exploring the wide range of possible blend configurations that might mimic this shallow signal is of the greatest interest for determining its true nature.

*Kepler* is likely to find many other candidate transiting planets similar to KOI-377.03, for which final validation by other means is not currently feasible, either because the expected radial-velocity signal is too small, or because Doppler measurements are otherwise complicated due to the star being chromospherically active, rapidly rotating, or too faint. With the application to KOI-377, we show that our light-curve modeling technique is a powerful tool for exploring astrophysical false positive scenarios that is complementary to other diagnostics, and should play an important role in the discovery of Earth-size planets around other *Kepler* targets.

## 2. SIMULATING FALSE POSITIVES WITH BLENDER

In general the detailed shape of a light curve displaying transit-like events can be expected to contain useful constraints on possible blend scenarios that might be responsible for those signals. With photometry of the quality of that provided by *Kepler*, those constraints can be quite strong, and may be used to exclude many blend configurations and provide support for the planetary hypothesis. It is thus highly desirable to take advantage of this information, particularly since it relies only on observations already in hand.

The idea behind **BLENDER** is to compare the transit photometry of a candidate against synthetic light curves produced by an eclipsing binary that is included within the photometric aperture of *Kepler*, and is contaminating the light of the candidate. The usually deep eclipses of the binary are attenuated by the light of the candidate, and reduced in depth so that they appear transit-like. In principle there is an enormous range of possible binary configurations that could mimic all of the features of true planetary transits, including not only their depth, but also the total duration and the length of the ingress and egress phases. Generally it is only with detailed modeling that these can be ruled out. Possible scenarios include not only background eclipsing binaries, but also hierarchical triples, i.e., an eclipsing binary physically associated with the candidate in a wide orbit around their common center of mass.

The basic procedure for simulating light curves with **BLENDER** was described in detail by Torres et al. (2004), and further changes and enhancements are discussed below. Briefly, the brightness variations of an eclipsing binary are generated with the binary light-curve code EBOP (Popper & Etzel 1981), based on the Nelson-

<sup>18</sup> For Earth-size planets, the amplitude of the signal in the *Kepler* band is very small and possibly below the detection threshold for *Spitzer*. However, a blend with a late-type binary could produce a much deeper eclipse at longer wavelengths that may be detectable in the near-infrared *Spitzer* bands.

Davis-Etzel model (Nelson & Davis 1972; Etzel 1981), and then diluted by the light of the candidate for comparison with the *Kepler* observations. Effects such as limb darkening, gravity brightening, mutual reflection, and oblateness of the binary components are included. The objects composing the binary are referred to as the ‘secondary’ and ‘tertiary’, and the candidate is the ‘primary’. The properties of each object needed to generate the light curves (brightness and size) are taken from model isochrones by Marigo et al. (2008), parametrized in terms of their stellar mass.<sup>19</sup> For the primary star the appropriate isochrone is selected by using as constraints the effective temperature, surface gravity, and metallicity determined spectroscopically. We assign also a mass and a radius from this isochrone, although these characteristics are irrelevant for generating the model light curves. We then read off the intrinsic brightness of the star (absolute magnitude) in the *Kepler* passband, which is the only property needed by BLENDER. The brightness of the primary is held fixed throughout all simulations. The parameters of the binary components are allowed to vary freely over wide ranges in order to provide the best match to the *Kepler* photometry in a chi-square sense, subject only to the condition that the two stars lie on the same isochrone, as expected from coeval formation. To read off their properties (absolute magnitude and size) we use the mass as an intermediate variable. The specific isochrone adopted for the binary depends on the configuration: for hierarchical triple scenarios we adopt the same age and chemical composition as the primary, whereas for background binaries the isochrone can be different. The *Kepler* light curve itself does not provide a useful constraint on the age or metallicity of the binary in the background case, so a typical choice is a model for solar metallicity and a representative age for the field such as 3 Gyr. For background binary scenarios the distance between the binary and the main star is parametrized for convenience in terms of the difference in distance modulus,  $\Delta\delta$ . The inferred distance between the primary star and the observer will vary from blend to blend because we constrain the combined brightness of all components of the blend to match the measured apparent brightness of the target. BLENDER is also able to account for differential extinction between the primary and the binary, which can have a non-negligible effect in some cases given the relatively low Galactic latitude of the *Kepler* field.

Early versions of BLENDER have been used occasionally in recent years to examine transiting planet candidates from ground-based surveys such as OGLE, TrES, and HATNet (see, e.g., Torres et al. 2004, 2005; Mandushev et al. 2005; O’Donovan et al. 2006; Bakos et al. 2007), as well as from CoRoT (Fressin et al. 2010). These studies have exploited the predictive power of BLENDER to estimate further properties of the blend

scenarios, by testing them against complementary information such as color indices, optical/near-infrared spectroscopy, or near-infrared photometry from *Spitzer*. For the application to *Kepler*, several important modifications have been made to BLENDER, including the following: *i*) the ability to generate light curves integrated over the 29.4-minute effective duration of an observation when using long-cadence data. This changes the shape of the transits significantly, given the high precision of the *Kepler* photometry and the relatively short timescales of the events (see Gilliland et al. 2010); *ii*) de-trending of the original *Kepler* light curves with a 1-day running median to remove instrumental effects, and rejection of outliers; *iii*) the use of model isochrones specific to the *Kepler* passband, kindly computed for us by L. Girardi. BLENDER can now also use proper limb-darkening coefficients for the same band, as opposed to an approximation to the *Kepler* passband such as the Johnson *R* filter, which is considerably narrower. *Kepler* limb-darkening coefficients have been computed by Sing (2010) and also A. Prsa;<sup>20</sup> *iv*) extension to any optical or near-infrared passband. In particular, for any scenario explored with BLENDER, light curves can be computed at other wavelengths such as the  $3.6\mu\text{m}$  and  $4.5\mu\text{m}$  passbands of the IRAC instrument on Warm *Spitzer*, in order to further test the blend hypothesis; *v*) the ability to have the tertiary be a (dark) planet instead of a star, in which case the corresponding free parameter becomes the radius of the planet rather than the tertiary mass. The mass of the planet has little effect on the light curves in most cases, but can nevertheless be set to any value;<sup>21</sup> *vi*) the ability to include extra light from other stars in the *Kepler* aperture, which further dilutes the intrinsic signatures from the eclipsing binary; *vii*) the ability to model systems with eccentric orbits. Eccentricity changes the orbital velocities during transit, and can therefore affect the size (mass) of stars that allow satisfactory fits to the light curve.

When exploring blend scenarios involving hierarchical triple systems, the free parameters of the problem are the mass of the secondary, the mass of the tertiary (or its radius, if a planet), and the inclination angle. A fourth variable, the difference in distance modulus, is added for background blends. These quantities are typically stepped over wide ranges in a grid pattern to fully map the  $\chi^2$  surface. For the application to KOI-377 below, stellar masses are allowed to vary along the isochrones between  $0.1 M_\odot$  and  $1.4 M_\odot$ , although at the larger values the observed duration of the transits is already difficult to match unless the events are highly grazing, in which case the shape would be very different. For planetary tertiaries the radii are allowed to be as large as  $1.8 R_{\text{Jup}}$ ; values higher than this have not been observed.

### 3. APPLICATION TO KOI-377

KOI-377 (KID 3323887, 2MASS 19021775+3824032) is a relatively faint star compared to typical ground-based transit hosts (*Kepler* magnitude  $K_p = 13.8$ ), which was

<sup>19</sup> This particular set of isochrones was chosen because it reaches lower masses than other models (nominally  $0.15 M_\odot$ , which we have extrapolated slightly for this application to  $0.10 M_\odot$ , near the brown dwarf limit), and because a convenient web tool provided by the authors allows easy interpolation in both age and metallicity (<http://stev.oapd.inaf.it/cgi-bin/cmd>). Additionally, isochrone magnitudes are available in a variety of passbands including the *Kepler* and *Spitzer* passbands, as well as Sloan and 2MASS.

<sup>20</sup> <http://astro4.ast.villanova.edu/aprsa/?q=node/8>

<sup>21</sup> We note that this option of BLENDER implicitly allows to consider white dwarfs as tertiaries, as they are also Earth-size and contribute no light. Their mass is significantly larger than a planet’s mass, however, which in close orbits can lead to distortions in the primary star causing ellipsoidal variation.

observed by the mission beginning in the first quarter of operations, and presents three distinct periodic signals in its light curve. The two with the largest amplitudes have periods of 19.24 days (*Kepler*-9 b) and 38.91 days (*Kepler*-9 c), and brightness decrements of 6.5 and 6.0 mmag, respectively. The third signal (KOI-377.03) is much shallower (0.2 mmag), and repeats every 1.59 days. The two longer periods are within 2.5% of being in a 2:1 ratio, and both objects display obvious TTVs that are anti-correlated, clearly indicating they are interacting gravitationally and therefore orbit the same star, and are planetary in nature (see Holman et al. 2010). The estimated radii are quite similar to that of Saturn, and the masses are somewhat smaller than Saturn, based on available radial-velocity measurements constrained by transit times and durations. The short-period signal has one of the smallest amplitudes detected by *Kepler*, and may well correspond to a third, super-Earth-size planet in the system, with an estimated radius of only  $1.4 R_{\oplus}$ . However, because it shows no TTVs related to the other two planets (nor is expected to, on dynamical grounds), and is predicted to induce only a very small reflex velocity on the parent star that may be below detection for such a faint object, the true origin of this signal has not yet been established.

In the absence of the crucial evidence of TTVs, each of the two largest signals—and indeed the third signal as well—could in principle be due to a different blend.<sup>22</sup> Therefore, as an illustration of the application of BLENDER, we model the light curve of KOI-377 at each period separately, as we would any candidate with a single period, and we account for possible blends at the other periods by incorporating extra dilution consistent with those other scenarios. The goal for the two largest signals is to demonstrate, as a sanity check, that BLENDER would be able to rule out blends in similar cases where confirmation is lacking, which *Kepler* is expected to find in significant numbers. For the third signal of unknown nature, the application of BLENDER should provide valuable evidence one way or the other.

### 3.1. Stellar properties and photometry

KOI-377 is a solar type star. The spectroscopic properties of the primary are adopted from Holman et al. (2010):  $T_{\text{eff}} = 5777 \pm 61$  K,  $\log g = 4.49 \pm 0.09$ , and  $[\text{Fe}/\text{H}] = +0.12 \pm 0.04$ . With these parameters, a comparison with the stellar evolution models of Marigo et al. (2008) yields a stellar mass of approximately  $M = 1.07 M_{\odot}$ , a radius of  $R = 1.02 R_{\odot}$ , and an age of about 1 Gyr, along with the absolute magnitude in the *Kepler* band. Only the latter is used by BLENDER, and is held fixed in our modeling. The distance to the star estimated from the same models is about 650 pc, ignoring extinction. Uncertainties in the brightness of the primary stemming from

errors in  $T_{\text{eff}}$ ,  $\log g$ , and  $[\text{Fe}/\text{H}]$  are small. For example, the error in  $\log g$ , which has the most direct influence on the intrinsic brightness, translates to an uncertainty of little more than 0.1 mag in the absolute magnitude. This has an insignificant impact on our results.

The photometry used here consists of the long-cadence measurements gathered for KOI-377 during *Kepler* quarters 1, 2, and 3, spanning 218 days, and was treated slightly differently than indicated earlier for a generic *Kepler* candidate because of the complications stemming from the TTVs. Using the binary FITS tables from MAST (Multimission Archive at STScI, <http://archive.stsci.edu/kepler/>), the “raw” aperture photometry for each quarter was first detrended using a moving cubic polynomial fit robustly to out-of-transit data, with a sliding window of 999 minutes before and after each individual datapoint. This technique removes long-term trends due to stellar activity or instrumental errors, but retains the properties of each transit light curve. Statistically significant outliers were removed.

For the two long-period signals, simple folding will not create an accurate light curve because of the strong TTVs. Instead, we used a “shift-and-stack” technique, in which each transit event is displaced so that it is centered at “time” zero using the measured transit times from Holman et al. (2010). Along with the measurements in transit, nearly a full cycle of out-of-transit data were also shifted. Specifically, we shifted nearly 25% of an orbital cycle before the transit, and nearly 75% after the transit. This preserves any curvature outside of eclipse, and in principle would also reproduce any secondary eclipses, both of which can provide useful constraints when modeling the light curve with BLENDER. We note, however, that the strong TTVs of the transits would be accompanied by shifted secondary eclipses in a way that can only be predicted by full numerical integration. This shift-and-stack technique would not align secondary eclipses correctly and thus their depth would need to be significant in each individual event to be noticed. There is no sign of secondary eclipses at these periods in the data at the  $10^{-4}$  level, as expected from the planetary nature of the objects, and thus the failure of the shift-and-stack technique to correctly add up the secondary eclipses does not affect our results. After shifting, all the transit and out-of-transit data were “stacked” together and each data point was given a time relative to time zero at the center of each transit event. This was done separately for the 19-day and 39-day signals. We have been careful not to use a full cycle of out-of-transit data to avoid using any photometric measurements more than once in the input light curve.

For the 1.6-day signal that repeats at regular intervals (since it shows no TTVs), we created a light curve by simply masking out the transits at the other two periods.

### 3.2. Additional observations for false positive rejection

The photometric aperture of *Kepler* is typically a few pixels across, with a scale of  $3''.98$  per pixel (see below). High-resolution imaging of KOI-377 was performed in order to identify neighboring stars that might be eclipsing binaries blended with and contaminating the target photometry. Images were recorded with the guider camera of the High Resolution Echelle Spectrometer (HIRES;

<sup>22</sup> Unlikely as it may seem to have three different blends operating in the same system, the large photometric aperture, nearly uninterrupted monitoring, very high photometric precision, and long-term coverage of *Kepler* coupled with the large number of targets observed makes it more sensitive to picking up odd cases such as this, so they should not be completely ruled out. An example already exists among the five multi-planet candidates recently reported by Steffen et al. (2010), in which one of the systems (KOI-191) presents three transit-like signals, and one of those signals (0.4 mmag depth) has been shown to be due to a background eclipsing binary 2.6 mag fainter than the target, located 1.5 arcsec away.

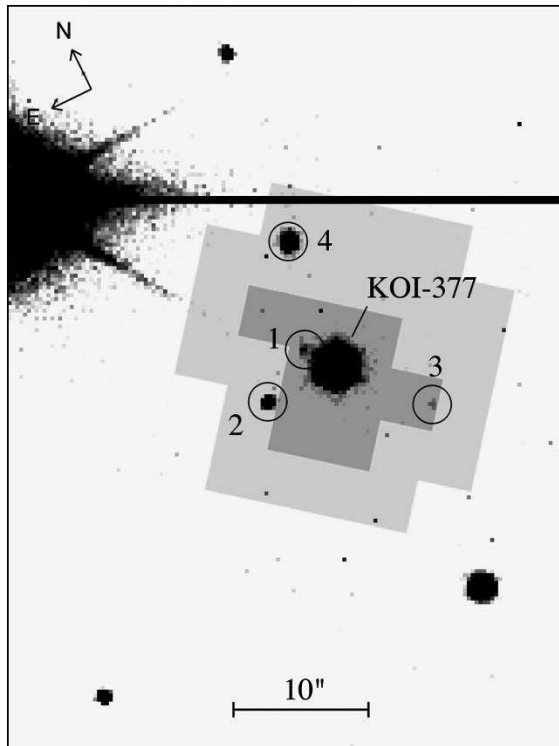


FIG. 1.— Image of KOI-377 from the HIRES guider camera on the Keck I telescope, obtained in seeing of  $0''.9$  and clear skies. Companions within  $15''$  are labeled as in Table 1. The scale of the image is  $0''.30 \text{ pix}^{-1}$ . Also indicated are the optimal photometric aperture (darker gray area of 8 pixels, used to extract the *Kepler* photometry) and the target aperture mask (lighter gray area of 31 pixels, used to measure centroids) for *Kepler* quarter 3.

Vogt et al. 1994) on the Keck I telescope on Mauna Kea, in unfiltered light. The nominal sensitivity of the CCD from 400 to 800 nm yields an effective passband similar to the *Kepler* passband. The field of view was  $43'' \times 57''$ , and the pixel scale was  $0''.30$  per pixel. One of these frames appears in Figure 1, and shows at least four stars in the field of view within  $15''$  of the target. Some of these stars are listed in various astrometric and photometric catalogs. The brightness of these companions relative to the target was measured using aperture photometry on four separate Keck images, and ranges from  $\Delta m = 2.6$  to  $5.9$  mag.

Speckle observations of KOI-377 were carried out on 2010 June 18 with the WIYN 3.5 m telescope located on Kitt Peak. They were taken with a two-color EMCCD speckle camera using narrow-band filters 40 nm wide centered at 562 nm and 692 nm. We refer loosely to these passbands as *V* and *R*. The native seeing was  $0''.7$ . No companions with  $\Delta m \leq 3.25$  mag (*R* band) are present in the field of view centered on the target out to  $1''.8$ , at the  $5\sigma$  confidence level. Inside of  $0''.2$  the sensitivity is reduced, but still allows to rule out brighter companions down to the diffraction limit of  $0''.04$ – $0''.05$  (see Figure 2). Details of the follow-up speckle observations in the context of the *Kepler* mission are described in more detail by Howell et al. (2010).

Additionally, KOI-377 was observed on 2010 July 2 at the Palomar Hale 200-inch telescope with the near-infrared adaptive optics (AO) PHARO instrument (Hayward et al. 2001), a  $1024 \times 1024$  Rockwell HAWAII HgCdTe array detector. Observations were made in the

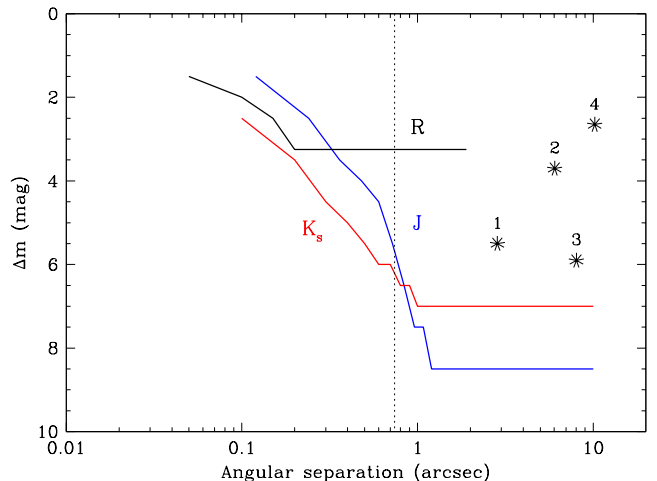


FIG. 2.— Sensitivity of our imaging observations to faint companions near KOI-377. Any companions above the curves are bright enough to be detected. *J* and *K<sub>s</sub>* limits are from AO observations at the Palomar 200-inch telescope, and *R* is from speckle observations using the WIYN 3.5 m telescope. Companions to the right of the vertical dotted line at  $0''.74$  cannot be responsible for the 1.6-day signal, as they would have induced centroid motion that is not observed. Stars detected in our imaging observations (Table 1) are marked with asterisks at their measured angular separations and magnitude differences in the *Kepler* passband.

*J* ( $1.25 \mu\text{m}$ ) and *K<sub>s</sub>* ( $2.145 \mu\text{m}$ ) bands. The field of view was approximately  $20'' \times 20''$ , and the scale was  $25.1 \text{ mas}$  per pixel. The AO system guided on the primary target itself, and produced Strehl ratios of 0.05 at *J* and 0.3 at *K<sub>s</sub>*. The central cores of the resulting point spread functions had widths of  $\text{FWHM} = 0''.12$  at *J* and  $\text{FWHM} = 0''.10$  at *K<sub>s</sub>*. The closer the companions seen earlier in the Keck images were easily detected, and we list them all in Table 1 along with relative positions, relative brightness estimates, and other identifications. The sensitivity to faint companions was studied by injecting artificial stars into the image at various separations and with a range of  $\Delta m$ , and then attempting to detect them both by eye and with an automated IDL procedure based on DAOPHOT. For firm detection we required the artificial stars to be present in both passbands. The sensitivity curves as a function of angular separation are shown in Figure 2, along with the *R*-band sensitivity estimated from the speckle observations.

Much fainter stars with  $\Delta m > 9$  near a *Kepler* target could in principle be detected by examining images from the Palomar Observatory Sky Survey, which date back more than 50 years, provided the proper motion of the target is large enough to have shifted it by several arc seconds over that period. This is not possible for KOI-377, since its total proper motion as reported in the UCAC2 Catalog (Zacharias et al. 2004) is only  $13.7 \text{ mas yr}^{-1}$ . The likelihood of such faint close-in companions must therefore be addressed statistically, if need be.

While the AO and speckle observations rule out the presence of bright neighboring stars as close as  $0''.1$  or slightly less, further limits on even tighter companions can be placed by the spectroscopic observations obtained with HIRES on the Keck I telescope, described by Holman et al. (2010), since those stars would fall well within the  $0''.86$  slit of the spectrograph. We performed simulations in which we added the spectrum of a faint star to the original KOI-377 spectra, over a range of rela-

TABLE 1  
COMPANIONS TO KOI-377 IDENTIFIED IN OUR IMAGING OBSERVATIONS.

Identification	SDSS coordinates (J2000)	$\rho$ ( $''$ )	P.A. (deg)	$\Delta J$ (mag)	$\Delta K_s$ (mag)	$\Delta K_p$ (mag)
KOI-377 <sup>a</sup>	19:02:17.76 +38:24:03.2	...	...	...	...	...
Comp 1 <sup>b</sup>	19:02:17.91 +38:24:05.4	2.85	37.9	6.84	6.84	5.5
Comp 2	19:02:18.27 +38:24:02.8	6.04	91.7	4.52	4.17	3.7
Comp 3	19:02:17.29 +38:23:57.1	8.03	221.8	6.25	6.04	5.9
Comp 4 <sup>c</sup>	19:02:17.69 +38:24:13.4	10.21	355.6	3.59	3.01	2.6

<sup>a</sup> Target is also known as 2MASS 19021775+3824032, KID 3323887, and *Kepler*-9.

<sup>b</sup> This companion is not listed in the SDSS catalog; the coordinates are inferred from its position relative to KOI-377.

<sup>c</sup> Also known as 2MASS 19021769+3824132 and KID 3323885.

tive brightnesses, and attempted to detect these artificial companions by examining the cross-correlation function. We estimate conservatively that any such stars with relative fluxes larger than about 10–15% ( $\Delta m$  less than 2 or 2.5 mag) would have been seen, unless their spectral lines are blended with those of the target. The sharp lines of KOI-377, with a measured rotational broadening of only  $v \sin i = 1.9 \pm 0.5 \text{ km s}^{-1}$ , make this rather unlikely.

### 3.3. Centroid analysis

Thanks to the very high astrometric precision of *Kepler*, an analysis of the motion of the photocenter of a target provides an effective way of identifying false positives that are caused by background eclipsing binaries falling within the aperture. The principles have been explained by Batalha et al. (2010) (see also Jenkins et al. 2010; Monet et al. 2010).

We describe first the use of difference image analysis based on data obtained during quarter 3 to demonstrate that the transit sources for all three KOI-377 planets and candidates are restricted to being very near the target star. A difference image is formed by averaging several exposures near, but outside of a transit and subtracting from this the average of all available exposures near transit center. This results in a typically isolated signal, a positive intensity with the shape of the point spread function (PSF) at the *true spatial location* of the transit source, and an amplitude equal to the photometric transit depth times the direct image intensity for the target. Adopting 40 independent transits of KOI-377.03 in quarter 3 (avoiding those shortly after major disturbances such as a safing event, and avoiding any that overlap with 'b' and 'c' transits) each formed with six symmetrically placed exposures outside of transits (after a two exposure gap) and three near transit minimum results in a 14- $\sigma$  signal in the difference image. The corresponding direct image is formed as the average of both in- and out-of-transit sets such that the direct and difference images are sums and differences of precisely the same exposure sets.

For *Kepler*-9b four transits were used from quarter 3 with five exposures in transit, a gap of three, then five more exposures on each side for out-of-transit. *Kepler*-9c used two transits with seven exposures in-transit, a gap of three, and seven symmetrically placed out-of-transit exposure blocks. By using only exposures pulled close in time, and symmetrically with respect to the transits in use to form a difference image, this effectively imposes a de-trending and avoids any complications from drifts on time scales longer than the average spread of

TABLE 2  
PRF CENTROID MEASUREMENTS ON KOI-377 DIRECT AND DIFFERENCE IMAGES.

Type	Intensity ( $e^-$ )	Column (pix)	Row (pix)	Radius offset (pix)
<i>Kepler</i> -9b				
Direct	$5.170 \times 10^7$	1099.6989	273.4557	
Difference	$4.360 \times 10^5$	1099.7058	273.4584	
S/N ; Offset	174	0.0069	0.0027	0.0074
Errors	2506	0.0029	0.0039	0.0049
<i>Kepler</i> -9c				
Direct	$5.132 \times 10^7$	1099.6999	273.4654	
Difference	$3.833 \times 10^5$	1099.7107	273.4990	
S/N ; Offset	128	0.0108	0.0336	0.0353
Errors	2991	0.0039	0.0056	0.0068
KOI-377.03				
Direct	$5.401 \times 10^7$	1099.6946	273.4408	
Difference	$1.493 \times 10^4$	1099.7131	273.4836	
S/N ; Offset	14.3	0.0185	0.0428	0.0047
Errors	1046	0.0351	0.0511	0.0062

NOTE. — The first two lines of each block present Intensity and two coordinate position PRF fit results for the Direct and Difference images, respectively. The third line shows the photometric signal-to-noise for the intensity in the Difference image, then the offset in position of the preceding two lines, with the last entry being the quadrature sum of the column and row offsets. Errors refer to the PRF fit to the Difference image.

the out-of-transit sets, which for *Kepler*-9c (the widest) is about 9 hours. Inspection of the difference images in Figure 3 shows that the transit sources for the confirmed 'b' and 'c' planets (Holman et al. 2010) and the candidate KOI-377.03 must arise from close to the target star, with offsets approaching one pixel easily ruled out by inspection. A weighted PSF fit (or more properly, a Pixel Response Function (PRF) fit; see Bryson et al. 2010) to each of the direct and three difference images of Figure 3 is formed using only the central  $3 \times 3$  pixel area centered on the brightest pixel. This leads to offsets with respect to 'b', 'c', and KOI-377.03 of 0.007, 0.035, and 0.047 pixels, respectively. For KOI-377.03 the formal error from a weighted least squares fit is 0.062 pixels. We have further assessed the errors by generating a large number of independent realizations of a transit signal of the KOI-377.03 relative intensity centered on the target coordinates. This leads to an *rms* scatter of 0.062 pixels. The noise had been increased by a factor of 1.2 in the difference image beyond direct Poisson plus readout noise estimates in order to yield this congruence of least-squares errors and scatter in simulations. The distribution of off-

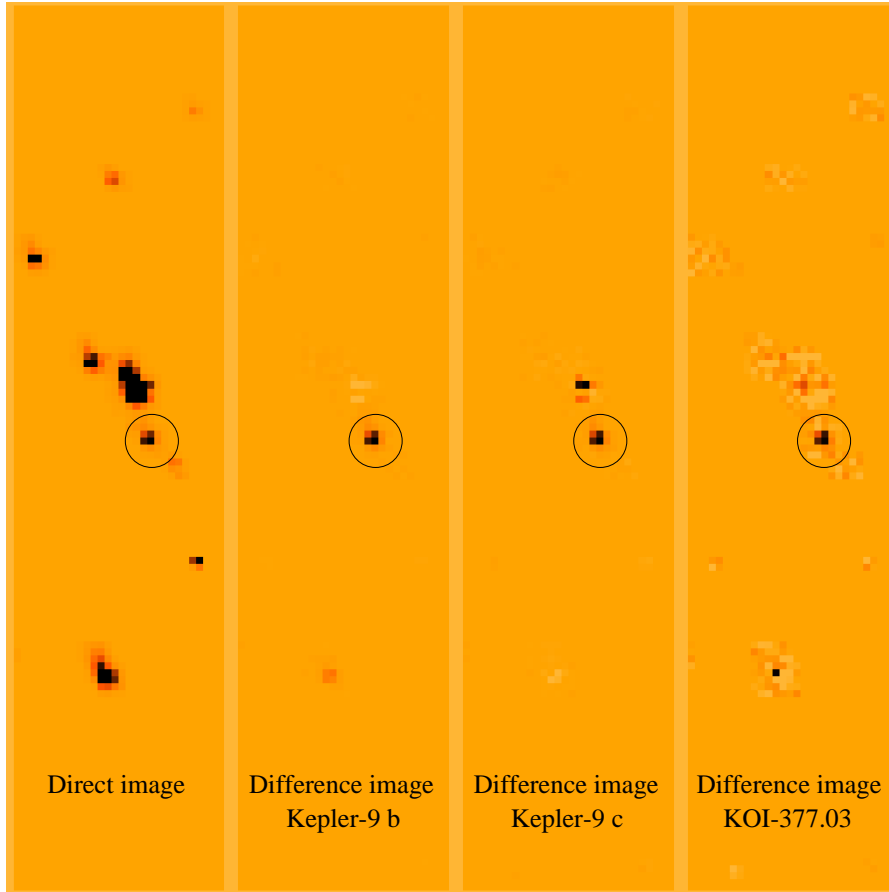


FIG. 3.— Direct and difference images for KOI-377. The four panels from left to right show 128 (row) by 30 (column) regions corresponding to the direct and difference images for planets ‘b’ and ‘c’, and candidate KOI-377.03. The pixels returned for all stars in this area have been mapped into original row and column locations on the detector. Over 90% of the image area is unfilled since *Kepler* returns only postage stamps on stars of interest. The target (KID 3323887) is indicated with circles in each panel. The locally brightest pixel is always at column 1100 and row 273, and each display panel has been normalized by the sum of counts within the  $3\times 3$  pixels centered on [1100, 273]. The display range is  $-0.03$  to  $0.3$ . The difference images were created to isolate the signals for transits ‘b’, ‘c’, and 377.03 respectively. Most stars, not having variations synced with these phases, effectively disappear in the difference images. For each of the three sets of transits the difference image in the  $3\times 3$  pixel core appears nearly identical to the direct image, demonstrating that the true transit source must be near the target to a small fraction of a pixel. The difference images also reflect the expected count levels for the source to be coincident with the target.

sets follows expected Gaussian statistics, e.g., in the 7472 trials for KOI-377.03 the extreme offset is  $4.2\sigma$  compared to the expected 4.0. We have also shown that simulating transit signals at 0.5 and 1.0 pixel offsets from the target results in similar and smaller statistical scatter, respectively, as less Poisson noise is under the transit image. We take the scatter of 0.062 pixels to generate a  $3\text{-}\sigma$  error circle of 0.186 pixels, or  $0''.74$ . This is the minimum radius within which background eclipsing binaries cannot be safely ruled out from centroid analysis of the *Kepler* data itself. To place this in perspective: centroid analysis has ruled out 98.6% of the area within the 8-pixel optimal aperture ( $>99.6\%$  of the 31-pixel mask) of Figure 1 as the location of potential background eclipsing binaries creating the KOI-377.03 signal.

The quantitative results for all three transit sets are given in Table 2. *Kepler-9 b* shows an offset of 0.0074 pixels between the difference and direct image relative to a  $1\text{-}\sigma$  error of 0.0049 pixels. A  $3\text{-}\sigma$  error circle in which background binaries cannot be excluded from the centroid analysis of *Kepler* data itself is only  $0''.06$ . *Kepler-9 c* is the only case of the three showing a formal

inconsistency with the offset being  $5\sigma$ ; however, even if we combine the offset and  $3\text{-}\sigma$  formal error any background eclipsing binaries outside of a radius of  $0''.22$  are excluded as the transit signal source. Clearly for all three transit sets, with the  $3\text{-}\sigma$  error circles comfortably under  $1''$  all of the known companions from high-resolution imaging shown in Table 1 are safely ruled out as sources of the photometric transit signal. It is worth noting that the formal (and equal to scatter from Monte-Carlo simulations) error on radial offsets is approximately equal in pixel units to the inverse photometric signal-to-noise (S/N) ratio, as expected (see, e.g., King 1983).

Further confirmation that the transits on KOI-377 are not due to known stars in the scene can be obtained via simulated transits placed on the known stars in KOI-377’s aperture compared with observation. This result is presented in detail for quarter 3 observations. Other quarters yield similar results.

The scene in the aperture is modeled using stars in the *Kepler* Input Catalog (KIC; Latham et al. 2005) supplemented by the stars in Table 1. To generate the modeled out-of-transit image, the measured PRF is placed



TABLE 3  
OBSERVED CENTROID SHIFTS FOR *Kepler-9 b*, *Kepler-9 c*, AND KOI-377.03.

	<i>Kepler-9 b</i>	<i>Kepler-9 c</i>	KOI-377.03
$\Delta R$	$2.22 \times 10^{-4} \pm 7.78 \times 10^{-5}$	$1.63 \times 10^{-4} \pm 9.34 \times 10^{-5}$	$3.71 \times 10^{-6} \pm 6.19 \times 10^{-5}$
$\Delta C$	$-2.25 \times 10^{-4} \pm 7.55 \times 10^{-5}$	$-2.57 \times 10^{-4} \pm 9.21 \times 10^{-5}$	$9.04 \times 10^{-6} \pm 5.82 \times 10^{-5}$
$D$	$3.16 \times 10^{-4} \pm 7.66 \times 10^{-5}$	$3.04 \times 10^{-4} \pm 9.25 \times 10^{-5}$	$9.77 \times 10^{-6} \pm 5.87 \times 10^{-5}$
$D/\sigma$	4.13	3.29	0.17

TABLE 4  
MODELED CENTROID SHIFTS DUE TO TRANSITS ON THE KNOWN STARS IN THE APERTURE WITH DEPTHS THAT REPRODUCE THE OBSERVED DEPTH.

Object	Modeled $D$	$D/\sigma$	Object	Modeled $D$	$D/\sigma$	Object	Modeled $D$	$D/\sigma$
<i>Kepler-9 b</i>	$1.21 \times 10^{-3}$	15.8	<i>Kepler-9 c</i>	$1.08 \times 10^{-3}$	11.7	KOI-377	$4.95 \times 10^{-5}$	0.84
Comp 1	depth > 1	...	Comp 1	depth > 1	...	Comp 1	$2.22 \times 10^{-4}$	3.77
Comp 2	$8.68 \times 10^{-3}$	113	Comp 2	$7.79 \times 10^{-3}$	84.2	Comp 2	$3.56 \times 10^{-4}$	6.07
Comp 3	depth > 1	...	Comp 3	depth > 1	...	Comp 3	$5.14 \times 10^{-4}$	8.76
Comp 4	$1.27 \times 10^{-2}$	165	Comp 4	$1.14 \times 10^{-2}$	123	Comp 4	$5.20 \times 10^{-4}$	8.85

NOTE. — For *Kepler-9 b* and *Kepler-9 c* transits on some companions can be ruled out because they require depth > 1.

at each star’s location on the focal plane, scaled by that star’s flux. This provides the contribution of each star to the flux in the aperture’s pixels. For each star  $s_i$  in the mask, the depth  $d_{s_i}$  of a transit that produces the observed depth is computed as the observed depth multiplied by the ratio of that star’s flux to the total observed flux. An in-transit image for each star in the aperture is modeled as in the out-of-transit image but with the star’s flux suppressed by  $1 - d_{s_i}$ .

A flux-weighted centroid is computed for the out-of-transit image and the in-transit-image generated for each star in the aperture. This produces row and column centroid offsets  $\Delta R$  and  $\Delta C$ , and the centroid offset distance  $D = \sqrt{\Delta R^2 + \Delta C^2}$ .

To compare these modeling results with observation we must make low-noise centroid measurements from the pixel data. We do this by creating out-of-transit and in-transit images from detrended, folded pixel time series. For each pixel time series, the de-trending operation has three steps: 1) removal of a 48-cadence median filtered time series; 2) removal of a robust low-order polynomial fit; and 3) the application of a Savitzky-Golay filtered time series of order 3 with a width of 10 cadences. The Savitzky-Golay filter is not applied within 2 cadences of a transit event, so the transits are preserved. The resulting pixel time series are folded by the transit period. Each pixel in the out-of-transit image is the average of 30 points taken from the folded time series outside the transit, 15 points on each side of the transit event. Each pixel in the in-transit image is the average of as many points in the transit as possible: seven for *Kepler-9 b* and *Kepler-9 c*, and four for KOI-377.03. Centroids are computed for the in-transit and out-of-transit images in the same way as the modeled images.

Uncertainties of these centroids are estimated via Monte Carlo simulation, where a noise realization is injected into 48-cadence smoothed versions of the pixel time series for each trial. A total of 2000 trials are performed each for *Kepler-9 b*, *Kepler-9 c*, and KOI-377.03. The in- and out-of-transit images are formed using the same de-trending, folding and averaging as the flight

data. The measured uncertainties are in the range of a few times  $10^{-5}$  pixels.

Table 3 shows the resulting measurements of the centroids from quarter 3 pixel data, along with the Monte-Carlo-based  $1\sigma$  uncertainties. The centroids are converted into centroid offsets and offset distance with propagated uncertainties. Table 4 shows the offset distance  $D$  predicted by the modeling method described above for each target in the aperture. While the modeled centroid shift when the transit is on KOI-377 is larger than the (expected) measured shift in all three cases, the centroid shift from modeled transits on companion stars is sufficiently large to rule out all of the known companions as the source of the transits.

### 3.4. BLENDER analysis of *Kepler-9 b* and *c*

As an initial test, we modeled the light curves for each of these two signals assuming they are the result of an eclipsing binary physically associated with the target, i.e., at the same distance (hierarchical triple). For this case the isochrone for the binary was taken to be the same as that of the primary, and corresponds to  $[\text{Fe}/\text{H}] = +0.12$  and an age of 1 Gyr. The secondary and tertiary masses were allowed to vary freely between  $0.10 M_\odot$  (the lower limit in the models; see footnote 19) and  $1.40 M_\odot$ , as mentioned earlier, seeking the best fit to the photometry. The inclination angle was also free, and the orbits were assumed to be circular. In both *Kepler-9 b* and *c*, which have similar transit signals, we find that the best fitting hierarchical triple blend model corresponds to secondaries that are approximately 1.0 and 0.5 mag fainter than the primary, respectively, and tertiaries that are at the lower limit of the isochrone range (late M dwarfs). However these fits give a poor match to the photometry: BLENDER is unable to simultaneously reproduce the total duration of the transit and the central depth, given the constraints on the brightness and size of the stars from the isochrones. This type of blend scenario is therefore clearly ruled out. We illustrate this for *Kepler-9 b* in Figure 4, where the best-fit planet model is also shown for reference. Much better matches to the data can be found



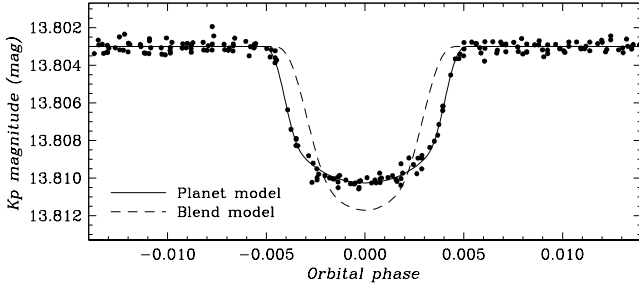


FIG. 4.— *Kepler* light curve of *Kepler-9b* ( $P = 19.24$  days) with the best fit blend model for the case of a hierarchical triple (candidate + physically associated eclipsing binary). The best fit planet model is shown for reference. The poor fit of the blend model rules out this configuration.

if additional light from a fourth star along the line of sight is incorporated into the model, providing extra dilution. We find that this fourth star is required to be nearly as bright as the primary, and the optimal model changes in such a way that the secondary also becomes as bright as the primary (so that its size enables the duration of the transits to be reproduced), while the tertiary remains a small star. This rather contrived scenario requiring two bright stars that are nearly identical to the main star would be easily recognized in our high-resolution imaging for separations larger than about  $0''.1$  (see, e.g., Figure 2), in our centroid analysis for separations larger than  $0''.06$ , or would otherwise produce obvious spectroscopic signatures unless all three bright objects happened to have the same radial velocity.

We next considered blends involving eclipsing binaries in the background, by removing the constraint on the distance. In this case a solar-metallicity isochrone was adopted for the binary, with a representative age for the field of 3 Gyr. We explored a wide range of relative distances, and we first considered main-sequence stars only, again with circular binary orbits. The results for *Kepler-9b* and *c* are once again similar to each other, and are illustrated for the second of these signals in Figure 5. The axes correspond to the distance modulus difference  $\Delta\delta$  as a function of the tertiary mass. Contours represent constant differences in the  $\chi^2$  of the fit compared to the best-fit planet model, and are labeled in units of the statistical significance of the difference ( $\sigma$ ). We draw two main results from this figure. One is that the light curve fits strongly prefer the smallest available tertiary masses from the isochrones ( $0.10 M_\odot$ ), and would in fact yield better fits for even smaller tertiary (i.e., planets). Additionally, the best solutions cluster toward equal distances for the binary and the primary star, effectively converging toward the equivalent of the hierarchical triple scenario considered earlier. No acceptable solutions exist with the binary at a significant distance behind the primary star. The best fit to the light curve of *Kepler-9c* is similar to the one shown in Figure 4 (dashed curve), which is not particularly good. The analogous diagram for *Kepler-9b* is qualitatively the same. Allowing the secondary to be a giant star gives a very poor fit to the photometry: the duration of the transit is very much longer than observed, there is out-of-eclipse modulation due to distortions in the giant, and all solutions place the binary at an implausibly large distance. We conclude that blend configurations involving background eclipsing binaries in which the tertiary is a star are not

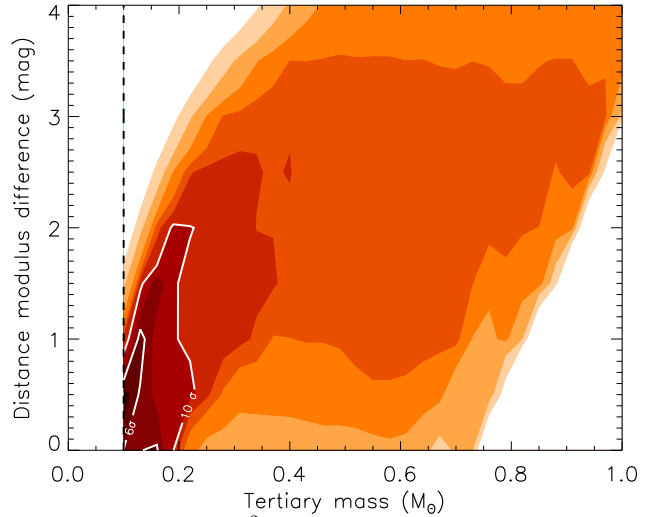


FIG. 5.— Map of the  $\chi^2$  surface (goodness of fit) corresponding to a grid of blend models for *Kepler-9c* ( $P = 38.91$  days) involving background eclipsing binaries with circular orbits. The separation between the binary and the primary is expressed in terms of the distance modulus difference. Contours are labeled with the  $\chi^2$  difference from the best planet model fit (expressed in units of the significance level of the difference,  $\sigma$ ), and are plotted here as a function of the mass of the tertiary star. The dashed line at  $0.1 M_\odot$  indicates the lower limit to the tertiary mass set by the model isochrones we use.

a viable explanation for either of these two signals.

We then explored background eclipsing binaries in which the tertiaries are planets rather than stars. This allows their radii to be smaller, possibly providing a better fit to the *Kepler* photometry. The orbits were considered to be circular, as before. Figure 6 shows the results for *Kepler-9c*, this time in the plane of separation versus secondary mass. Once again the fits tend to favor an equal distance for the binary and the primary star, and background scenarios with the binary far behind provide unacceptably poor matches to the light curve. A second noteworthy result is that these solutions have a strong preference for secondary stars that are quite similar to the primary. All acceptable fits to the light curve correspond to relatively bright secondaries with  $\Delta Kp < 1.5$  mag (see Figure 6). The best of these solutions is of about the same quality as a planet model, and has a secondary of mass  $0.98 M_\odot$  that is only 100 K cooler and 0.3 mag fainter than the primary in the *Kepler* band. This somewhat artificial case of “twin” stars is a result we have seen often in simulations for other *Kepler* candidates. The tertiary in this type of blend solution comes out about  $\sqrt{2}$  larger than in a planet model because the transit is diluted by another star of approximately equal size and brightness. One may debate whether this situation should actually be referred to as a “false positive” for KOI-377, since the signal would still correspond to a gas giant planet, only that this planet would be  $\sqrt{2}$  larger, and it would be orbiting a different star. Alternatively, it could be thought of simply as an overlooked dilution factor in a true planetary system. In any event, the lack of evidence for this bright twin star in the spectroscopy or in our high-resolution imaging or centroid analysis for KOI-377 does not support this scenario.

As a particular case of this family of configurations, we examined blends in which the star-planet pair is constrained to be at the same distance as the primary, i.e.,

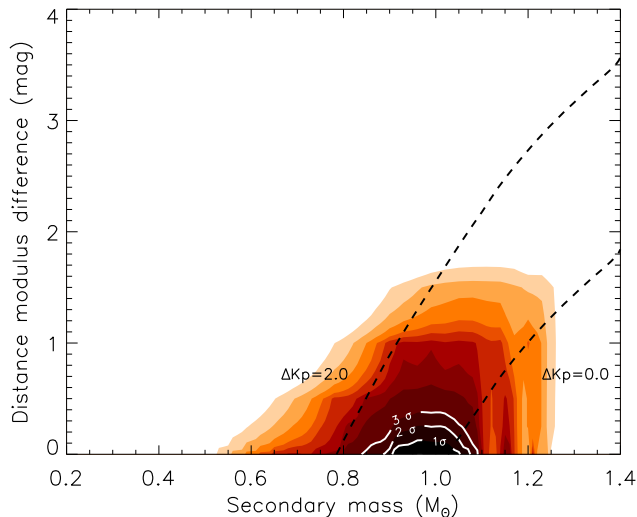


FIG. 6.— Map of the  $\chi^2$  surface corresponding to a grid of blend models for *Kepler-9c* involving background eclipsing systems in which the tertiary is a (dark) planet, in a circular orbit around the secondary. Contours are labeled with the  $\chi^2$  difference from the best planet model fit (expressed in units of the significance level of the difference,  $\sigma$ ). Two dashed lines of equal magnitude difference ( $\Delta Kp$ ) are indicated, and show that all viable blend fits (with confidence level  $< 3\sigma$ ) have secondaries that are bright enough to have been detected spectroscopically ( $\Delta Kp < 2$ ).

effectively in a hierarchical system. The secondary properties were therefore taken from the same isochrone as the primary, and the orbits were assumed to be circular. An excellent fit to the light curve is possible for a tertiary that is about  $\sqrt{2}$  larger than in a true planet model, but not surprisingly, we find once more that the secondary must be as bright as the primary.

Additional tests were run to examine the impact of changing the age adopted for the isochrone of the secondary in a background star-planet pair, or the addition of light from a fourth object in the aperture. In the first case, changing the age from 3 Gyr to 1 Gyr produced a small shift of the contours in Figure 6 downward and to the right that is simply due to the change in intrinsic brightness of the secondary star, and does not alter our conclusions. Adding “fourth light” further attenuates the eclipses of the star-planet pair. To compensate, *BLENDER* requires a slightly deeper eclipse, and in order to preserve the shape of the signal (total duration, and slope of ingress/egress), this is achieved by bringing the secondary closer to the primary. As a result, for relatively bright fourth light the contours are shifted downward by approximately the difference in magnitude between the primary and the fourth star, again without changing the conclusions.

One may also imagine blend scenarios in which the eclipsing binary is in the foreground, rather than the background. We explored this possibility by extending the simulations to negative values of  $\Delta\delta$ . As before, we adopted circular orbits and a 3 Gyr isochrone for the foreground system. Binaries with stellar tertiaries are clearly ruled out as they yield fits to the light curve that do not match its shape, and additionally they predict a fairly obvious secondary eclipse that is not seen in the data. We focus therefore on blends in which the tertiary is a planet, and we illustrate the results for *Kepler-9c*. In this case we find there are many acceptable solutions with  $\chi^2$  values differing from the best planet fit at the

level of  $1\sigma$  or less. These solutions span a range of secondary masses and a range of foreground separations, implying a wide range not only in apparent brightness for the secondary, but also in color. Models in which the secondaries are brighter than the primary and of significantly different spectral type would be inconsistent with the spectroscopic parameters derived for KOI-377, and are excluded. Plausible solutions remain, in principle, for fainter foreground secondaries, which necessarily involve later-type stars. We find that of these, the only ones that yield acceptably good fits to the *Kepler* photometry, with  $\chi^2$  values differing from the planet fit by less than  $3\sigma$ , correspond to secondaries that are within about 1.5 mag of the primary in brightness, and are of course redder. These would be valid blend configurations so long as the secondaries are close enough to the primary to be spatially unresolved (angular separations  $\lesssim 0''.1$ ), and at the same time faint enough to have gone undetected in the spectra. Stars that are within  $\sim 2$ – $2.5$  mag of the primary would generally have been seen spectroscopically, as indicated in Sect. 3.2, and this would exclude these remaining foreground blend configurations. Nevertheless, to be conservative, let us assume for the moment that a star 1.5 mag fainter than the primary has still managed to elude detection in our spectra. This corresponds to the faintest secondary in a foreground blend scenario that still allows for a satisfactory fit to the light curve, and would be the most difficult case of this kind to disprove. This fit is shown in the top panel of Figure 7, and is statistically indistinguishable from a planet model fit. The secondary in this configuration is an M2 dwarf ( $M = 0.56 M_\odot$ ) 1.53 mag fainter than the primary, eclipsed by a  $0.91 R_{\text{Jup}}$  planetary companion, and is located at a distance of 300 pc. The primary in this scenario is at 750 pc.

Other properties of this particular blend such as magnitudes and colors can be computed easily with *BLENDER*, and compared with observations. Apparent magnitudes for KOI-377 are available from the KIC for a variety of passbands including Sloan *griz*, a special-purpose passband referred to as D51 (centered on the Mg Ib triplet at 518.7 nm), and *JHK<sub>s</sub>* from the 2MASS catalog. The lower panel of Figure 7 shows various color indices ( $Kp - \lambda$ ) predicted by *BLENDER* both for the primary star alone and for the blend. Those of the primary are well reproduced by the model, and we find that a small amount of interstellar extinction leads to an even better match (solid line in the figure). The colors of the blend, on the other hand, disagree with the measured colors, and deviate by more than 0.4 mag for the reddest index,  $Kp - K_s$ . We are therefore able to exclude, solely on the basis of its color, this most difficult of the scenarios involving foreground star-planet pairs that could mimic the 19-day and 39-day signals in the light curve of KOI-377. Larger-mass secondaries would not be as red and still allow for good fits to the photometry, but they are intrinsically brighter and would be recognized more easily.

The above simulations have all assumed circular orbits for the blended eclipsing binaries or star-planet pairs, which is not necessarily realistic given the relatively long periods of *Kepler-9b* and *c*. Eccentricity affects the speed of the secondary and tertiary in their relative orbit, and therefore can change the duration of the tran-

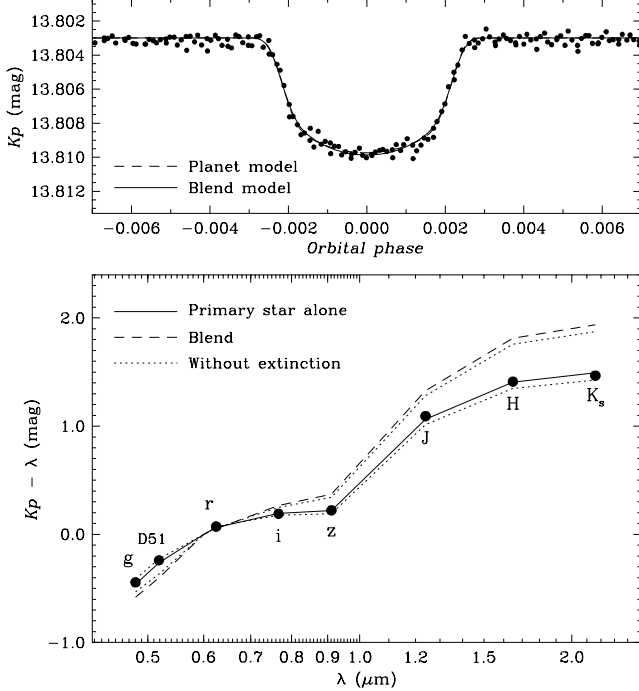


FIG. 7.— *Top*: Light curve of *Kepler-9c* with the best fit blend model for the case of contamination by a foreground eclipsing pair with a circular orbit in which the tertiary is a planet. The pair consists of an M2 dwarf ( $0.56 M_{\odot}$ ,  $0.58 R_{\odot}$ ) and a  $0.91 R_{\text{Jup}}$  companion 450 pc in front of the primary, which is at 750 pc. This fit is statistically indistinguishable from best fit planet model, also shown for reference. *Bottom*: Measured colors for KOI-377 (dots) compared with the predictions from the blend model in the top panel. A small amount of extinction ( $0.15 \text{ mag kpc}^{-1}$ ) has been included in these predictions. The results without considering extinction differ little, and are shown with dotted lines. The color measurements clearly rule out such a blend.

sit, making it shorter or longer than in a circular orbit, depending on the orientation (longitude of periastron,  $\omega$ ). It also changes the impact parameter, all else being equal. And finally, it shifts the location of the secondary eclipse. The magnitude of these effects is illustrated in Figure 8 for eccentricities between 0.1 and 0.7. The most important effect for our purposes is on the transit duration. Given a fixed (measured) duration, eccentric orbits may allow blends with smaller or larger secondary stars than in the circular case to still provide satisfactory fits to the light curve, effectively increasing the pool of potential false positives. The limiting cases correspond to  $\omega = 90^\circ$  and  $270^\circ$ , in which the line of apsides is aligned with the line of sight and the transit occurs at periastron (accommodating larger secondaries) or apastron (smaller secondaries), respectively. Extensive simulations for these two extreme situations show that allowing for eccentric orbits does not change our conclusions regarding hierarchical triple systems, background eclipsing binaries, or background star-planet scenarios. We show this for the latter blend category in Figure 9, illustrated for the case of orbits with eccentricities of 0.3 and 0.5, and  $\omega = 90^\circ$ . Comparison with Figure 6 indicates that in both cases the blends are still bright enough that we would have seen signatures of them in the spectra of KOI-377. Larger eccentricities of  $e = 0.7$  result in secondaries that are brighter still. For eccentric orbits oriented such that transits take place at apastron ( $\omega = 270^\circ$ ), we only find acceptable fits to the light curves for eclipsing

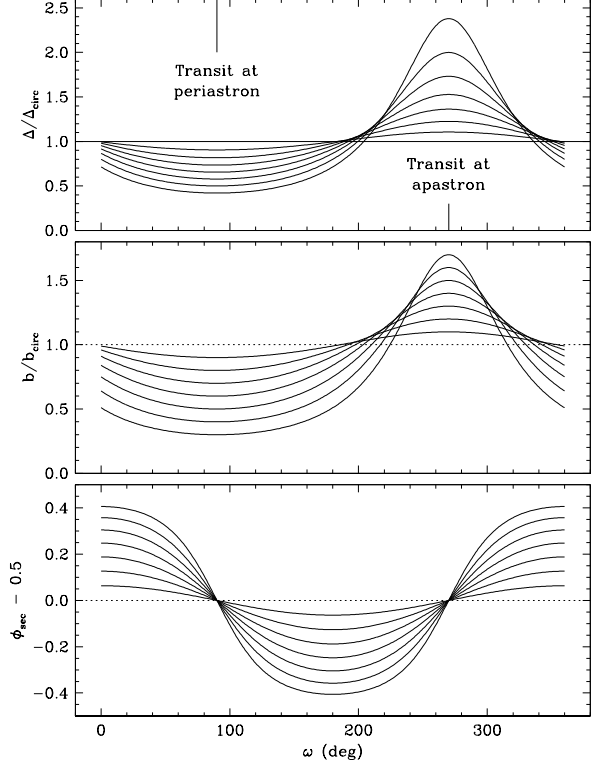


FIG. 8.— Effect of eccentricity on the duration of transits relative to the circular orbit case ( $\Delta/\Delta_{\text{circ}}$ ), on the impact parameter ( $b/b_{\text{circ}}$ ), and on the displacement of the secondary eclipses relative to phase 0.5 ( $\phi_{\text{sec}} - 0.5$ ), all shown as a function of the longitude of periastron  $\omega$ . The different curves correspond to eccentricities from 0.1 to 0.7 in steps of 0.1.

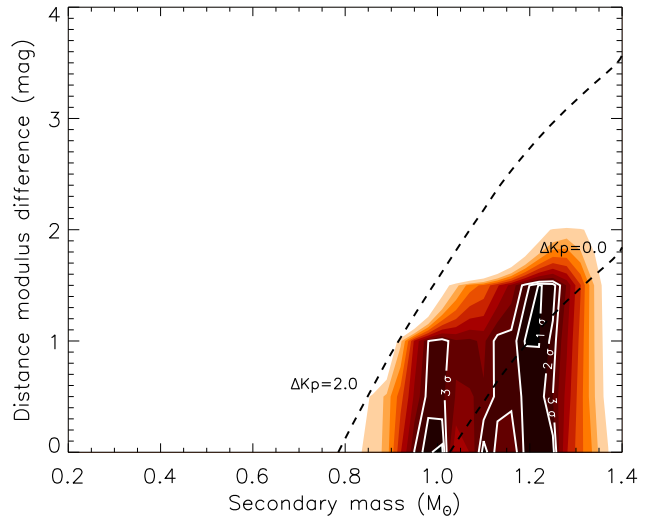


FIG. 9.— Same as Figure 6 (*Kepler-9c*), restricted to star-planet orbits having  $e = 0.3$  (concentration of contours on the left) and 0.5 (right), and  $\omega = 90^\circ$ . This orientation corresponds to transits that occur at periastron. Comparison with Figure 6 shows that these solutions allow for more massive (larger) secondary stars than in the case of circular orbits, but the brightness of these blends is still within 2 magnitudes of the target, and is ruled out by spectroscopy.

star-planet pairs that are in the foreground (and involve smaller stars). However, as was the case for circular orbits, those blends are either too bright, too red, or both, and are thus also excluded.

The above, fairly exhaustive exploration of parameter space with BLENDER allows us to conclude that no configuration involving an eclipsing binary (or an eclips-

TABLE 5  
SUMMARY OF BLEND CONFIGURATIONS TESTED FOR *Kepler*-9 B AND C.

False positive configuration <sup>a</sup>	Result	Blends ruled out
Hierarchical triple with stellar tertiary, MS		
• Circular and eccentric orbits.....	poor fits/sec.ecl.	Yes
• Added fourth light .....	twin star	Yes (imaging/spec./centr.)
Hierarchical triple with planetary tertiary, MS		
• Circular and eccentric orbits.....	twin star	Yes (imaging/spec./centr.)
Background EB with stellar tertiary		
• Circular and eccentric orbits, MS and giants .....	poor fits	Yes
Background EB with planetary tertiary, MS		
• Circular and eccentric orbits.....	twin star	Yes (imaging/spec./centr.)
• 1 Gyr isochrone for secondary .....	little change	Yes (imaging/spec./centr.)
• Added fourth light .....	little change	Yes (imaging/spec./centr.)
Foreground EB with stellar tertiary, MS		
• Circular and eccentric orbits.....	poor fits/sec.ecl.	Yes
Foreground EB with planetary tertiary, MS		
• Circular and eccentric orbits.....	too bright/too red	Yes (imaging/spec./centr./color)

<sup>a</sup> 3 Gyr isochrone assumed for background and foreground stars, unless otherwise indicated. Abbreviations: MS = main sequence secondary; imaging/spec./centr. = high-resolution imaging, spectroscopy, and centroid analysis; sec.ecl. = secondary eclipses predicted but not observed; EB = eclipsing binary.

ing star-planet pair), either in the foreground or in the background, is able to provide a reasonable explanation for the signals of *Kepler*-9 b and c (see Table 5 for a summary of the configurations tested, and the results). Many scenarios lead to light curves that match the detailed shape of the transit events, but none are simultaneously consistent with all of the other observational constraints. This includes spectroscopy, high-resolution imaging, centroid measurements, and photometry (colors). Therefore, even ignoring the evidence from TTVs, these results fully support the planetary nature of these objects and demonstrate the usefulness of BLENDER for validating transiting planet candidates from *Kepler*.

### 3.5. BLENDER analysis of KOI-377.03

We proceed next to examine false positive scenarios for the shallowest signal in KOI-377, with  $P = 1.59$  days. Because the period is so short in this case, and tidal forces in such binary systems have likely circularized the orbit, we do not consider non-zero eccentricities. As for the larger signals, hierarchical triple systems in which the tertiary is a star fail to provide good fits to KOI-377.03. A good match to the *Kepler* photometry can be found when the tertiary is allowed to be a much smaller planet, but as was the case earlier, it requires a secondary that is very similar to the primary in brightness. The resulting size of the eclipsing planet is  $\sqrt{2}$  larger than in a planet model, or about  $2 R_{\oplus}$ . This type of configuration was ruled out earlier based on the high-resolution imaging and the spectroscopy.

Blends with an eclipsing binary in the background (the tertiary being a star) are able to reproduce the light curve just as well as a planet model. In Figure 10 we illustrate those results by showing the area of allowed parameter space in a diagram of distance modulus difference as a function of secondary mass. Acceptable fits with  $\chi^2$  differing from the planet model by less than  $3\sigma$  are possible over a wide range of relative separations ( $4.5 \leq \Delta\delta \leq 9$ ), but the secondaries are restricted to a relatively narrow interval in mass centered on the mass of the primary.

These eclipsing binaries are all very distant and faint ( $Kp \approx 19$ –22), and have no effect on the colors of the blend. The more distant scenarios place the binary at implausibly large distances of up to 42 kpc (more than 10 kpc above the Galactic plane). The nearest configuration ( $\Delta\delta = 4.5$ ; see Figure 10) has the binary at a distance of 5.3 kpc, and the primary at  $\sim 670$  pc. The secondary in this model is a late G star 5.5 mag fainter than the primary in the *Kepler* passband, eclipsed by a late M dwarf that produces no detectable secondary eclipse. The predicted brightness of this binary precisely matches that of the closest companion identified in the AO images (Comp 1, Table 1), located  $2''.85$  NE of the target. However, this and all wider visual companions are already ruled out at more than the  $3\sigma$  confidence level by the lack of centroid motion, which would have

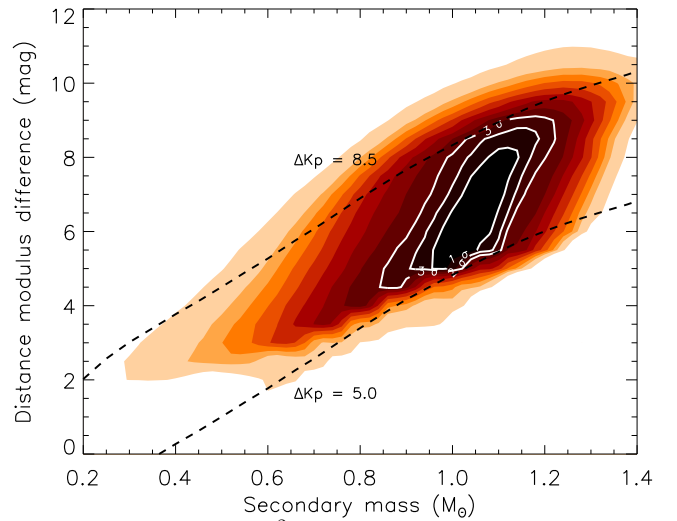


FIG. 10.— Map of the  $\chi^2$  surface for KOI-377.03 corresponding to a grid of blend models involving background eclipsing binaries with stellar tertiaries. Contours are labeled with the  $\chi^2$  difference from the best planet model fit (expressed in units of the significance level of the difference,  $\sigma$ ). The dashed lines indicate levels of equal apparent magnitude difference  $\Delta Kp$  between the background binary and the primary star.



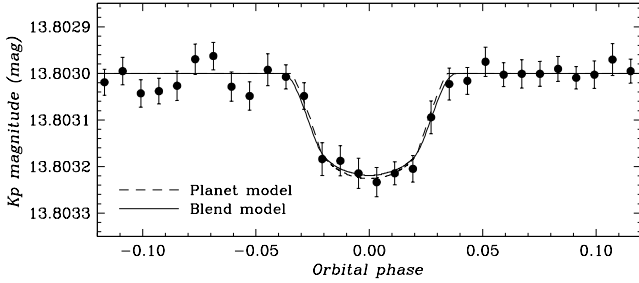


FIG. 11.— Example of a blend model fit to KOI-377.03 involving a background eclipsing binary with a stellar tertiary (solid line). The secondary is similar in spectral type to the primary and 5.2 mag dimmer, and the tertiary is a late M dwarf. The eclipsing pair is 6 kpc behind the primary. This fit is statistically indistinguishable from the best fit planet model, which is shown with a dashed line. The *Kepler* observations have been binned for clarity.

revealed any blended eclipsing binaries at angular separations larger than about  $0''.74$  (Sect. 3.3). Even without this constraint from astrometry, the predicted  $J-K_s$  color of the secondary in this blend is considerably redder than measured for this close AO companion, which would also disqualify it. Eclipsing binaries that are between 5 and  $\sim 8.5$  magnitudes fainter than the main star provide acceptably good fits to the light curve (see Figure 10), and if they were angularly closer than  $0''.74$  from the target they may not be detectable in our AO or speckle observations, in our centroid motion analysis, nor in our spectra. They remain viable blend configurations, and would necessarily be at distances greater than 5 or 6 kpc. An example is shown in Figure 11, to illustrate that the fit is indistinguishable from a planet fit.

In the above calculations we have ignored interstellar extinction. However, given the large distances for the binaries in some of these blend configurations, it is worth exploring the effect of dust more carefully, which we have done by repeating the BLENDER simulations using a representative differential extinction coefficient of  $0.5 \text{ mag kpc}^{-1}$ . The results are shown in Figure 12, and indicate that the blend scenarios providing good fits to the *Kepler* photometry of KOI-377.03 are systematically shifted to smaller distances compared to the previous calculations. Their apparent brightness, however, changes relatively little, as can be seen by comparing the lines of equal  $\Delta Kp$  with those in Figure 10. Therefore, the overall impact of differential extinction on the permitted area of parameter space in terms of observable parameters is not as significant as might have appeared.

Allowing the tertiary to be a planet opens up a different area of parameter space for permissible background blends (Figure 13). When including extinction as before, acceptable fits to the light curve are possible for  $\Delta\delta$  values from zero up to about 4.5. This upper limit corresponds to distances for the star-planet pair of about 4.8 kpc (with  $\Delta Kp \approx 6$ , or apparent magnitudes of  $Kp \approx 20$ ), and is set by the maximum size of  $1.8 R_{\text{Jup}}$  we have allowed for a planet. As in the configurations described before, the solutions constrain the secondary masses to be near that of the primary in order to match the detailed shape and observed duration of the transits, with a range from about  $0.9 M_{\odot}$  to  $1.2 M_{\odot}$ . Therefore, the color of the blend is not as useful a discriminant in this case. Secondaries that are less than about 2 mag fainter than the primary would have been seen spectroscopically. This excludes a good fraction of the space

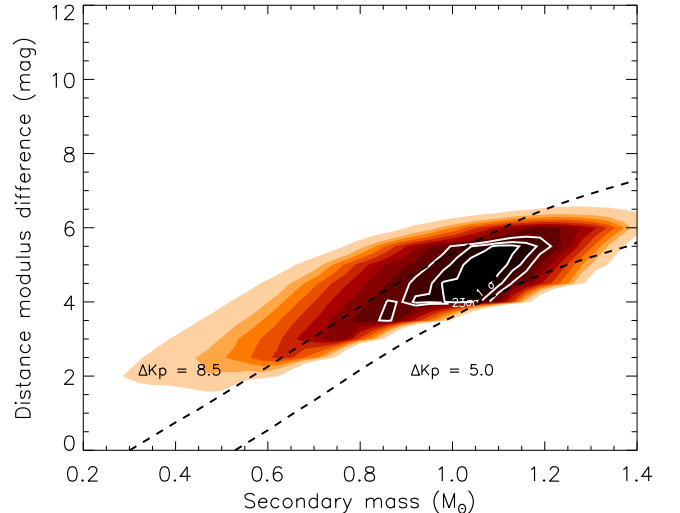


FIG. 12.— Same as Figure 10, including the effect of differential extinction in the amount of  $0.5 \text{ mag kpc}^{-1}$ . The net effect of extinction is to compress and shift the contours toward smaller relative distances. The dashed lines indicate levels of equal apparent magnitude difference  $\Delta Kp$  between the background binary and the primary star, and are the same as shown in Figure 10.

of parameters, as indicated by the lower dashed line in Figure 13. Of the remaining blends of this kind between  $\Delta Kp = 2$  and  $\Delta Kp = 6$ , only the ones with angular separations smaller than about  $1''$  are allowed by the constraints from our AO imaging (see Figure 2), but the centroid analysis is even more restrictive and rules out stars outside of  $0''.74$ . At closer separations, the high-resolution images rule out all blends that are brighter than the sensitivity limit indicated in the figure (i.e., those that fall above the curves).

As expected from the fixed duration and depth of the transit-like signal of KOI-377.03, the size of the tertiary in these configurations correlates with the secondary mass. Due to this correlation, small tertiaries with  $R \lesssim 0.3 R_{\text{Jup}}$  (roughly Neptune-size, and smaller) are further excluded because the eclipses they produce are already very shallow, and further dilution by the

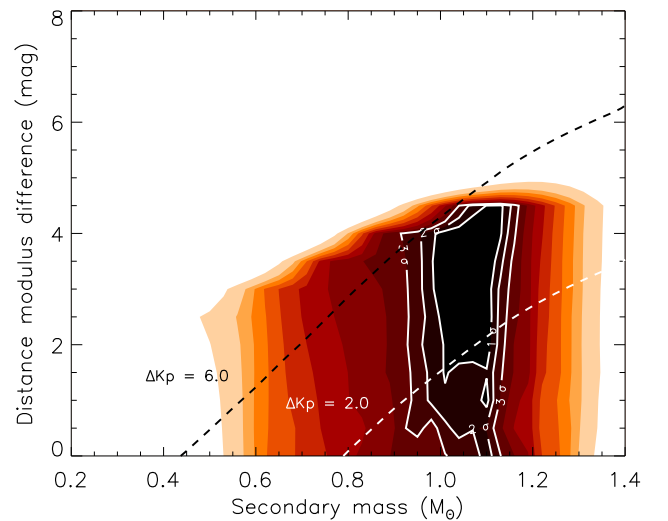


FIG. 13.— Same as Figure 12, but for the case in which the tertiary is a planet instead of a star. Differential extinction is included. Kinks in the contours are an artifact of the discreteness of our grid. The dashed lines indicate levels of equal apparent magnitude difference  $\Delta Kp$  between the background secondary and the primary star. The lower of these lines represents the constraint from the spectroscopy for KOI-377 (see text).

primary would make them too shallow to fit the photometry. In order to avoid this, the secondaries in those blends must be relatively small late-G type stars that are nearby, and would therefore be bright enough ( $\Delta Kp \lesssim 2$ ) that they would have been detected in our spectra as a second set of lines. Thus, BLENDER effectively places limits not only on the secondary, but also on the size of the tertiary (see Figure 14). In particular, blends with a white dwarf eclipsing a background star are also ruled out for the same reason described above. Many of the larger tertiaries correspond to gas giants (Saturn-size, or larger), which implies a qualitative difference in their nature compared to the alternate model of a true Earth- or super-Earth-size planet. In this sense these blends may properly be considered “false positives”, as opposed to the configurations discussed earlier requiring twin stars, which only change the tertiary radius by  $\sqrt{2}$ .

Finally, we examine the possibility that the true period of the KOI-377.03 signal is twice the nominal value. Alternating events would then correspond to the primary and secondary eclipses of a blended eclipsing binary (the tertiary being a star in this case), which may in general be of different depth. In KOI-377.03 there is no compelling evidence for a depth difference between odd- and even-numbered events, but this is difficult to establish in a faint star such as this for a signal that is only 0.2 mmag deep. The results of extensive simulations with BLENDER for this scenario are illustrated in Figure 15. The best fits correspond to blended binaries far in the background, and do not indicate a significant difference in depth between the primary and secondary eclipses. However, these fits provide only a poor representation of the *Kepler* light curve, and can therefore be confidently ruled out. This is seen in Figure 16. The top panel shows the closest fit to the full light curve together with the data, and in the bottom panel we have binned the measurements to facilitate the comparison. This solution involves an eclipsing pair of mid-G dwarfs at 21 kpc and 7.2 mag fainter than the primary, and the fit is visibly worse than that corresponding to a planet at half the

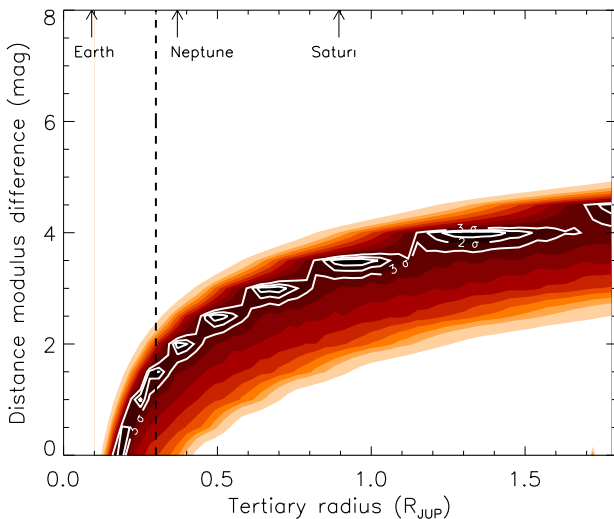


FIG. 14.— Same as Figure 13, shown here as a function of the tertiary radius. Kinks in the contours and closed inner contours for the 1- $\sigma$  and 2- $\sigma$  levels are an artifact of the discreteness of our grid. We indicate with a dashed line the lower limit for the size of the tertiaries that is set by the spectroscopic constraint on presence of bright stellar companions (see text). The size of the Earth, Neptune, and Saturn are also indicated for reference.

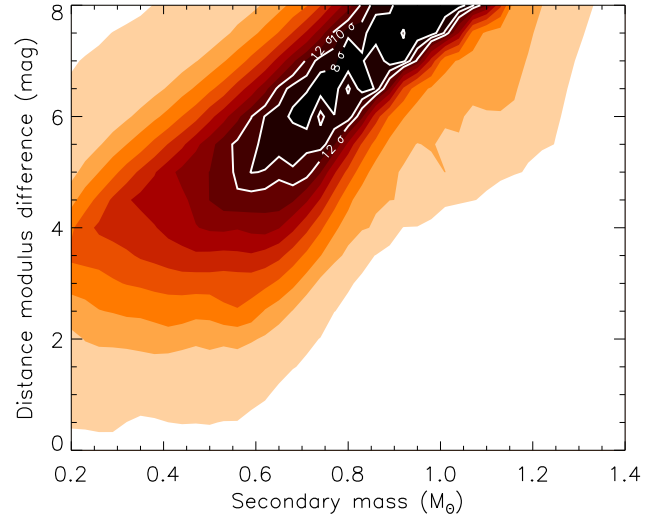


FIG. 15.— Same as Figure 10, but for the case in which the orbital period is assumed to be twice the nominal value ( $2P = 3.1850$  days).

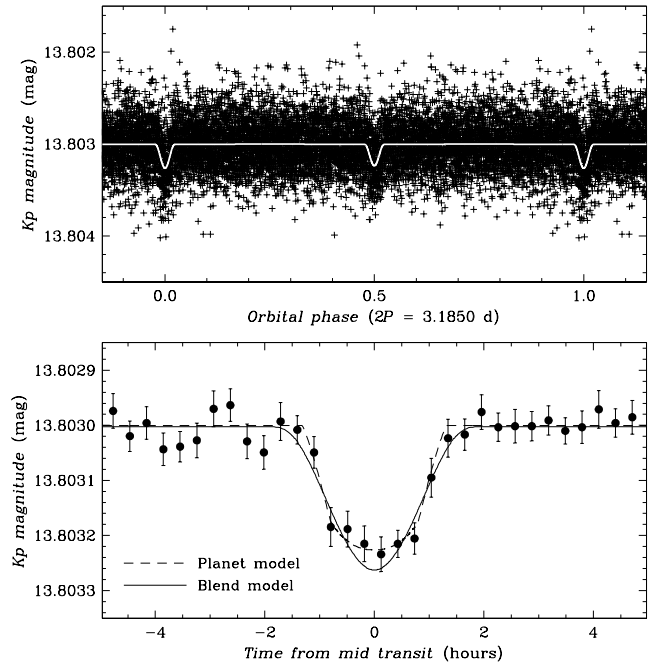


FIG. 16.— Blend model of a background eclipsing binary with twice the nominal period of KOI-377.03. *Top*: *Kepler* observations and best blend fit corresponding to two nearly equal mid G dwarfs eclipsing each other, and located 20.4 kpc behind the primary. *Bottom*: Binned observations compared against the blend model in the top panel. The fit corresponding to a planet model is shown for reference.

period, which is shown with the dashed line.

In summary, the BLENDER analysis of this section coupled with constraints from spectroscopy, high-resolution imaging, and centroid motion measurements rules out a large fraction of the false positives that could produce the 1.6-day signal, but not all (see Table 6). The remaining configurations involve background stars that are similar to the primary in spectral type (late F to early K, or about  $0.9 M_{\odot}$  to about  $1.2 M_{\odot}$ ), and are eclipsed either by another smaller star or by a planet with  $R_p > 0.3 R_{\text{Jup}}$  (Neptune-size or larger). These blends range in apparent brightness from  $Kp \approx 19$  to  $Kp \approx 22$  for stellar tertiaries, and from  $Kp \approx 16$  to  $Kp \approx 20$  if the tertiaries are plan-

TABLE 6  
SUMMARY OF BLEND CONFIGURATIONS TESTED FOR KOI-377.03.

False positive configuration <sup>a</sup>	Result	Blends ruled out
Hierarchical triple with stellar tertiary, MS.....	poor fits	Yes
Hierarchical triple with planetary tertiary, MS.....	twin star	Yes (imaging/spec./centr.)
Background EB with stellar tertiary, MS		
• With and without extinction .....	good fits	Not all
• Twice the period .....	poor fits/sec.ecl.	Yes
Background EB with planetary tertiary, MS		
• Jupiters, Neptunes, super-Earths, with extinction....	good fits	super-Earths
• White dwarfs, with extinction .....	good fits	Yes (imaging/spec./centr.)
Foreground EB with stellar tertiary, MS.....	poor fits	Yes
Foreground EB with planetary tertiary, MS.....	poor fits	Yes

<sup>a</sup> 3 Gyr isochrone assumed for background and foreground stars, unless otherwise indicated. Orbits are circular. Abbreviations: MS = main sequence secondary; imaging/spec./centr. = high-resolution imaging, spectroscopy, and centroid analysis; sec.ecl. = secondary eclipses predicted but not observed; EB = eclipsing binary.

ets, and must be closer than  $0''.74$  from the target. At separations under  $0''.74$  our imaging observations allow us to rule out the brighter of these blends, and only the ones with  $\Delta m$  below the sensitivity curves in Figure 2 would remain undetected.

### 3.6. Likelihood of remaining blend scenarios for KOI-377.03

In order to provide the basis for an estimate of the confidence level for the planetary status of KOI-377.03, we describe here the calculation of the likelihood that the signal is due to a background blend involving either a stellar tertiary or a planetary tertiary, taking into account the constraints on brightness and other properties indicated in the previous section. Because this type of calculation is likely to be relevant for other *Kepler* candidates, we describe it here in some detail.

The frequency of stars in the mass range permitted by BLENDER was estimated using the Besançon Galactic structure models of Robin et al. (2003), specifically for the *R* band, which is the closest available to the *Kepler* passband. We used an aperture of 1 square degree centered on KOI-377, and we performed the calculations in half-magnitude bins of apparent brightness, accounting for interstellar extinction as we did in the BLENDER simulations, with a coefficient of  $0.5 \text{ mag kpc}^{-1}$  in *V*. The range of allowed secondary masses for each magnitude bin was taken directly from Figure 12 for blends with stellar tertiaries, and from Figure 13 for blends with planetary tertiaries.

Using the density of stars for each magnitude bin, we calculated the fraction that would remain undetected after our high-resolution imaging (speckle and AO observations), spectroscopy, and centroid motion analyses. The results are listed in Table 7. The first two columns give the *Kp* magnitude range of each bin and the magnitude difference  $\Delta Kp$  compared to the target, calculated at the upper edge of the magnitude bins. For convenience the calculations for blends with stellar tertiaries and planetary tertiaries are listed separately. For the stellar tertiary case, column 3 reports the density of stars obtained from the Besançon models, restricted to the mass range allowed by BLENDER as shown in Figure 12. Column 4 lists the maximum angular separation  $\rho_{\text{max}}$  at

which stars in the corresponding magnitude bin would go undetected in our imaging observations, read off from Figure 2, and taken at the center of each magnitude bin. Centroid motion analysis rules out eclipsing binaries beyond  $0''.74$ , so  $\rho_{\text{max}}$  is constant at that value for the last few bins in which this provides a stronger constraint than the imaging. The total number of stars of the appropriate mass range in a circle of radius  $\rho_{\text{max}}$  around KOI-377 is then given for each bin in column 5, in units of  $10^6$ .

The intrinsic frequency of eclipsing binaries in the field is a key ingredient in the calculation, and for this we have relied on the results of Prsa et al. (2010), which are based on the *Kepler* observations themselves. These authors found the average occurrence rate of eclipsing binaries among the *Kepler* targets down to *Kp*  $\approx 16$  to be approximately 1.2% across the entire field. This may be a slight overestimate because it counts as variables stars that are actually blended with a background binary that is not a target, though the effect is likely small. There is little information available on fainter eclipsing binaries, so we assume here that a similar frequency holds. More importantly, many of these eclipsing binaries cannot produce signals such as that of KOI-377.03 because their light curves have the wrong shape. Examples include contact binaries and ellipsoidal variables, in which the brightness changes continuously throughout the cycle, rather than presenting sharp transit-like events such as we observe. Additionally, semi-detached systems would have eclipses that are too long and also of the wrong shape. We therefore exclude these from the tally. With this adjustment, the frequency of eclipsing binaries capable of producing blends is 0.53%. Multiplying the star counts in column 5 by this frequency, we obtain the total number of blends expected in each magnitude bin, which is reported in column 6.

Columns 7–9 are similar to columns 3–5, but for blends involving star-planet pairs. Note that the range of allowed magnitudes is different in this case, as is the range of secondary masses used to compute the densities in column 7 (see Figure 13). Following the size ranges adopted by Borucki et al. (2010b), we consider three categories of transiting planets as potential companions: super-Earths ( $1.25\text{--}2 R_{\oplus}$ ), Neptune-size planets ( $2\text{--}6 R_{\oplus}$ ), and Jupiter-size planets ( $6\text{--}22 R_{\oplus}$ , or equivalently  $\sim 0.5\text{--}2.0$



$R_{\text{Jup}}$ ). Planets smaller than  $0.3 R_{\text{Jup}} = 3.4 R_{\oplus}$  are ruled out by BLENDER, as they can only reproduce the light curve if the secondaries are relatively bright, but those would have been detected spectroscopically. This effectively eliminates all super-Earths, and a fraction of the Neptunes. For the intrinsic frequency of transiting planets we have relied on the results from the first 33 days of *Kepler* observations as reported by Borucki et al. (2010b). That census is unlikely to have missed many Neptune- or Jupiter-size planets (except ones with very long periods), although it may include false positives, so we consider the count to be conservative. Those authors presented a list of 306 transiting planet candidates, and described another 400 candidates that have not yet been released. Of the 306 candidates, 24% would correspond to Jupiter-size planets, and 23% to Neptune-size planets. One may reasonably assume that the 400 sequestered targets contain a larger fraction of smaller Earth- or super-Earth-size planets (which cannot mimic the light curve of KOI-377.03; see Sect. 3.5), for at least two reasons. Smaller planets are the main focus of the *Kepler* mission, and they require more intensive follow-up efforts for validation, which is why those targets have not yet been made public. Secondly, these 400 targets are brighter, which makes smaller planets around them easier to detect. Consequently, the assumption of similar Jupiter- and Neptune-size planet frequencies as given above, but for the entire sample of 306+400 targets showing transit-like features, is a conservative one. Scaling to the full sample of 156,097 *Kepler* targets (Borucki et al. 2010b), we find an upper limit to the frequency of transiting Jupiter-size and Neptune-size planets of 0.11% and 0.10%, respectively.<sup>23</sup> With these adopted frequencies, the resulting numbers of blends involving these types of planets are listed in columns 10 and 11 of Table 7.

The total blend frequencies in each of columns 6, 10, and 11 are calculated as the sum of the individual frequencies in each magnitude bin, and the three columns are then combined in the bottom section of the table to yield an overall blend frequency (BF) of  $\sim 1.0 \times 10^{-7}$ .

This very small figure corresponds to the number of false positives we expect to find *a priori* around KOI-377.03. This does not translate directly into a false alarm probability, or equivalently into a confidence level that the candidate is orbited by a true super-Earth-size planet, however, since that requires knowledge of the rate of occurrence of such planets. For a random candidate star in the field the rate of false positives relative to the rate of true planets (false alarm rate, FAR) can be written quite generally as  $\text{FAR} = N_{\text{FP}}/(N_{\text{FP}} + N_p)$ , where  $N_{\text{FP}}$  is the number of false positives and  $N_p$  is the number of planets in the sample. Thus, the larger the number of planets we expect, the smaller the FAR.

We consider KOI-377 to be fairly representative of a

typical target in the field in terms of its spectral type (solar), brightness, and background stellar density (a function of Galactic latitude). In that case, the total number of blends can be taken to be approximately the product of BF and the size of the sample, or  $N_{\text{FP}} = \text{BF} \times 156,097 = 0.016$ . The number of small planets expected in the sample is of course not known, and determining it is precisely one of the goals of the *Kepler* mission. Nevertheless, it is possible to make educated guesses as to the rate of occurrence of these objects in several ways, if only to have a rough approximation of what the confidence level would be. In order to be conservative, our estimates of  $N_p$  (or the corresponding frequency  $f_p$ ) should be *lower* limits.

In order to make an initial assessment of the odds ratio that KOI-377.03 is a super-Earth-sized planet rather than an astrophysical false positive, we consider multiple estimates for the rate of super-Earth-sized planets, drawing on both theoretical and observational considerations. Firstly, theoretical models such as those of Ida & Lin (2004) and Mordasini et al. (2009) based on the formation of planets by the core accretion process and subsequent migration have made predictions for the frequency of planets by mass and orbital separation. These models suggest that the frequency of planets of mass one to several Earth-masses is either similar to or larger than the frequency of Neptune-mass or Jupiter-mass planets. While the mapping between planet mass and planet radius is non-trivial, these models suggest that the frequency of transiting super-Earth-size planets could be roughly the same as or even larger than the frequency of transiting giant planets (which is  $\sim 0.1\%$ ).

Secondly, we can estimate the relative rates for small planets based on the *Kepler* results themselves. Among the 306 candidates reported by Borucki et al. (2010b), 27 fall in the category of super-Earths by size ( $R_p \leq 2 R_{\oplus}$ ). If we assume conservatively that these are the only transiting super-Earth-size planets in the *Kepler* field, ignoring any that might be present among the 400 targets that are not yet public, then we arrive at a small-planet frequency of  $f_p \approx 1.7 \times 10^{-4}$ . This may still be an overestimate, of course, if a significant fraction of the 306 publicly released planet candidates turn out to be false positives. While we have demonstrated above that the rate of false positives (BF) for KOI-377.03 is quite low, most stars have not received a similar level of scrutiny of follow-up observations and analysis. Given the disparate level of vetting of the various candidates, a rigorous analysis is beyond the scope of this paper.

We note that the above estimate of the rate of small planets based on *Kepler* observations,  $f_p \approx 1.7 \times 10^{-4}$ , is significantly smaller than that based on theoretical models ( $f_p \approx 10^{-3}$ ). To be conservative, we estimate the false alarm rate for KOI-377.03 using both the lower rate estimate ( $f_p \approx 1.7 \times 10^{-4}$ ) and an alternative rate which has been arbitrarily reduced by an order of magnitude ( $f_p \approx 1.7 \times 10^{-5}$ ). In the latter case, the number of small planets in the entire *Kepler* sample would be only  $N_p \sim 2.7$ . With these assumptions, the false alarm rate for KOI-377.03 being a false positive would be  $\text{FAR} \approx 0.016/(27 + 0.016) = 5.9 \times 10^{-4}$  using the higher value of  $f_p$ , and  $\text{FAR} \approx 0.016/(2.7 + 0.016) = 5.9 \times 10^{-3}$  using the lower  $f_p$ . Either of these rates implies that KOI-377.03 is most likely a super-Earth-size planet, rather than one of the false positives considered in this paper.

<sup>23</sup> As a check we may compare the above frequency of transiting Jupiter-size planets against results from the statistical study by Fressin et al. (2009). These authors combined the findings of various radial-velocity searches and folded-in the detections of very short-period systems detected by ground-based transit surveys, which are typically less common in Doppler searches. They found that 0.074% of solar-type stars have a transiting Jupiter-size planet. Our upper limit of 0.11% is consistent with this, given the presumably higher completeness of *Kepler* and the fact that a fraction of the *Kepler* candidates that is yet to be determined may turn out to be false positives once the follow-up is completed.

## 4. DISCUSSION

The calculation of the false alarm rate for KOI-377.03 described in the previous section,  $\text{FAR} \approx 5.9 \times 10^{-3}$  if we use our smallest estimate of  $f_p$ , is believed to be on the conservative side, based on current knowledge. It depends crucially on this frequency of small transiting planets, which may only be fully known at the conclusion of the *Kepler* mission. While it is therefore not possible to be certain that our  $f_p$  is an absolute lower bound, and that FAR is an upper bound, the results as they stand are compelling in suggesting a high likelihood that the 1.6-day signal is not due to a false positive. For an adopted stellar radius of  $1.02 R_\odot$  for the primary star, the estimated size of this planet would be approximately  $1.4 R_\oplus$ , which is the smallest yet reported.<sup>24</sup> A mass determination for this object has not been made, and will be challenging given the small amplitude expected for the reflex motion of the star, which would be only  $1.4 \text{ m s}^{-1}$  assuming a similar density as the Earth. Velocity measurements are further complicated by the presence of the other two planets in this system.

Many of the most interesting candidates found by *Kepler* will correspond to Earth-size planets, some of which are expected to be in the habitable zone of their host star. For solar-type stars this implies reflex motions with radial-velocity amplitudes below current detection limits, making the spectroscopic measurement of the mass impossible. Other reasons may also hinder this type of validation, such as rapid rotation, chromospheric activity, or even the faintness of the star.

The information contained in the *Kepler* light curves on the shape of a transit-like event is a valuable asset for constraining the vast range of possible astrophysical false positives that might be masquerading as a planet. Here we have shown how modeling the light curve of a candidate directly as a false positive allows to rule out a significant fraction of blends involving background or foreground eclipsing binaries or star-planet pairs, as well as hierarchical triple systems, each of these possibly attenuated by the light of additional stars. The combination of BLENDER with follow-up observations consisting of high-resolution imaging, spectroscopy, and an analysis of the centroid motion of the target leaves no room for a false positive in the case of KOI-377 b and c. These

signals were previously known to correspond to bona-fide Saturn-size planets because they display correlated TTVs (Holman et al. 2010). Nevertheless, the exercise serves to show that, lacking that evidence, it would still be possible to validate them using the same techniques, thus validating the general approach and justifying the application to the more interesting KOI-377.03 signal.

Among the advantages of BLENDER for *Kepler* is the ability to predict the brightness and overall color of a blend in many different passbands. Brightness information for virtually every *Kepler* target is available from the KIC in the Sloan *griz* and 2MASS *JHK<sub>s</sub>* bands, as well as in the custom D51 passband (518.7 nm). We have shown earlier how these can be used to rule out certain blend scenarios that might otherwise be viable. The detailed fitting of the photometry with a false-positive model provides additional discriminating power. Rough estimates of the properties of a background eclipsing binary that can mimic a blend have sometimes been made in previous transit surveys based simply on the apparent brightness of the object and a representative depth for its undiluted eclipses (such as 50%). While such systems may well reproduce the observed amplitude of a candidate light curve, not much can be said about the expected shape, which may be completely wrong. An example of this is seen for KOI-377.03 in Figure 16, in which a back-of-the-envelope calculation of the depth one might predict from the brightness and  $\sim 50\%$  deep eclipses of this binary may not be far off, but the detailed shape is not a good match to the observations, and BLENDER easily rules out this configuration giving a poor  $\chi^2$  for the fit. Without these additional constraints on blend properties provided by the detailed light-curve fitting, the space of parameters open to false positives would be significantly larger, and more difficult to exclude by other means.

Funding for this Discovery mission is provided by NASA's Science Mission Directorate. We are grateful to Leo Girardi for computing isochrones for this work in the *Kepler* passband, to Frédéric Pont for very helpful discussions on false alarm probabilities, and to David Sing for advice on limb-darkening coefficients.

Charbonneau et al. 2009).

## REFERENCES

- Bakos, G. Á. et al. 2007, *ApJ*, 670, 826  
 Batalha, N. M. et al. 2010, *ApJ*, 713, L103  
 Borucki, W. J. et al. 2010a, *Science*, 327, 977  
 Borucki, W. J. et al. 2010b, submitted (arXiv:1006.2779)  
 Bryson, S. T. et al. 2010, *ApJ*, 713, L97  
 Charbonneau, D. et al. 2009, *Nature*, 462, 891  
 Etzel, P. B. 1981, in *Photometric and Spectroscopic Binary Systems*, eds. E. B. Carling and Z. Kopal (Dordrecht: Reidel), 111  
 Fressin, F. et al. 2010, in preparation  
 Fressin, F., Guillot, T., & Natta, L. 2009, *A&A*, 504, 605  
 Gilliland, R. L. et al. 2010, *ApJ*, 713, L160  
 Hayward, T. L., Brandl, B., Pirger, B., Blacken, C., Gull, G. E., Schoenwald, J., & Houck, J. R. 2001, *PASP*, 113, 105  
 Holman, M. J. et al. 2010, *Science*, in press  
 Howell, S. et al. 2010, in preparation  
 Ida, S., & Lin, D. N. C. 2004, *ApJ*, 604, 388  
 Jenkins, J. et al. 2010, *ApJ*, in press (arXiv:1001.0416)  
 King, I. R. 1983, *PASP*, 95, 163  
 Koch, D. G. et al. 2010, *ApJ*, 713, L79  
 Latham, D. W., Brown, T. M., Monet, D. G., Everett, M., Esquerdo, G. A., Hergenrother, C. W. 2005, *BAAS*, 207, #110.13  
 Léger, A. et al. 2009, *A&A*, 506, 287  
 Mandushev, G. et al. 2005, *ApJ*, 621, 1061  
 Marigo, P., Girardi, L., Bressan, A., Groenewegen, M. A. T., Silva, L., & Granato, G. L. 2008, *A&A*, 482, 883  
 Monet, D. G., Jenkins, J. M., Dunham, E. W., Bryson, S. T., Gilliland, R. L., Latham, D. W., Borucki, W. J., & Koch, D. G. 2010, arXiv:1001.0305  
 Mordasini, C., Alibert, Y., & Benz, W. 2009, *A&A*, 501, 1139  
 Nelson, B., & Davis, W. 1972, *ApJ*, 174, 617  
 O'Donovan, F. T. et al. 2006, *ApJ*, 644, 1237  
 Popper, D. M., & Etzel, P. B. 1981, *AJ*, 86, 102  
 Prsa, A. et al. 2010, *ApJ*, submitted (arXiv:1006.2815)  
 Queloz, D. et al. 2001, *A&A*, 379, 279

- Robin, A. C., Reyl  , C., Derri  re, S., & Picaud, S. 2003, *A&A*, 409, 523
- Sing, D. K. 2010, *A&A*, 510, 21
- Steffen, J. H. et al. 2010, *ApJ*, submitted (arXiv:1006.2763)
- Torres, G., Konacki, M., Sasselov, D. D., & Jha, S. 2004, *ApJ*, 614, 979
- Torres, G., Konacki, M., Sasselov, D. D., & Jha, S. 2005, *ApJ*, 619, 558
- Vogt, S. S. et al. 1994, *Proc. SPIE*, 2198, 362
- Zacharias, N., Urban, S. E., Zacharias, M. I., Wycoff, G. L., Hall, D. M., Monet, D. G., & Rafferty, T. J. 2004, *AJ*, 127, 3043

TABLE 7

BLEND FREQUENCY ESTIMATE FOR KOI-377.03 BASED ON STELLAR DENSITIES AND FREQUENCIES OF ECLIPSING BINARIES AND TRANSITING PLANETS.

$Kp$ range (mag)	$\Delta Kp$ (mag)	Blends involving stellar tertiaries				Blends involving planetary tertiaries				
		Stellar density per sq. deg	$\rho_{\max}$ ( $''$ )	Stars ( $\times 10^6$ )	EBs $f_{\text{EB}} = 0.53\%$ ( $\times 10^6$ )	Stellar density per sq. deg	$\rho_{\max}$ ( $''$ )	Stars ( $\times 10^6$ )	Transiting Jupiters $6-15 R_{\oplus}, f_{\text{Jup}} = 0.11\%$ ( $\times 10^6$ )	Transiting Neptunes $3.4-6 R_{\oplus}, f_{\text{Nep}} = 0.10\%$ ( $\times 10^6$ )
(1)	(2)	(3)	(4)	(5)	(6)	(7)	(8)	(9)	(10)	(11)
13.8–14.3	0.5	...	...	...	...	...	...	...	...	...
14.3–14.8	1.0	...	...	...	...	...	...	...	...	...
14.8–15.3	1.5	...	...	...	...	...	...	...	...	...
15.3–15.8	2.0	...	...	...	...	...	...	...	...	...
15.8–16.3	2.5	...	...	...	...	563	0.14	2.675	0.0029	0.0027
16.3–16.8	3.0	...	...	...	...	595	0.17	4.168	0.0046	0.0042
16.8–17.3	3.5	...	...	...	...	588	0.20	5.701	0.0063	0.0057
17.3–17.8	4.0	...	...	...	...	430	0.23	5.514	0.0061	0.0055
17.8–18.3	4.5	...	...	...	...	292	0.25	4.424	0.0049	0.0044
18.3–18.8	5.0	2	0.35	0.059	0.0003	125	0.35	3.712	0.0041	0.0037
18.8–19.3	5.5	14	0.45	0.687	0.0036	57	0.45	2.798	0.0031	0.0028
19.3–19.8	6.0	14	0.55	1.027	0.0054	24	0.55	1.760	0.0019	0.0018
19.8–20.3	6.5	20	0.70	2.376	0.0126	...	...	...	...	...
20.3–20.8	7.0	13	0.74	1.726	0.0091	...	...	...	...	...
20.8–21.3	7.5	3	0.74	0.398	0.0021	...	...	...	...	...
21.3–21.8	8.0	4	0.74	0.531	0.0028	...	...	...	...	...
21.8–22.3	8.5	0	0.74	0.000	0.0000	...	...	...	...	...
22.3–22.8	9.0	0	0.74	0.000	0.0000	...	...	...	...	...
Totals		70	...	6.804	<b>0.0359</b>	2674	...	30.752	<b>0.0339</b>	<b>0.0308</b>
Blend frequency (BF) = $(0.0359 + 0.0339 + 0.0308) \times 10^{-6} = 1.006 \times 10^{-7}$										